nitrosylcobalt, dicarbonylnitrosylpryidylcobalt, nitric oxide, nitrous oxide, nitrogen oxide, nitrosyl chloride, and carbon monoxide were identified by their characteristic infrared bands. Nitrogen dioxide gas reacted with the potassium chloride cell windows to form potassium nitrate and nitrosyl chloride. Potassium nitrate has a sharp infrared absorption band at 1350 cm^{-1} which remained after cell evacuation. Nitrosyl chloride decomposed in the beam to yield nitric oxide and chlorine gas. Nitrosyl chloride reacts photochemically with $Co(CO)_3NO$ to produce NO_2 but no N_2O. The black powdered products from the photolysis of nitrosyltricarbonylcobalt in the presence of argon, nitrogen, and hydrogen were analyzed for cobalt content according to literature procedures.[32] In each case approximately 90 ± 10% of the material was cobalt.

Solid photoproduct from the reaction with hydrogen chloride was analyzed for cobalt[32] and chlorine[33] content according to literature procedures. Anal. Calcd for $CoCl_2$: Co, 45.4; Cl, 54.6. Found: Co, 45.3; Cl 54.4. For production of the solid photoproducts, a 500-cm^3 vessel containing about 50 μL of $Co(CO)_3NO$ was used.

The cell used for the gas phase ionic conductivity examination of the excited state was a modification of that used for relative quantum yield determinations. Electrodes consisted of 1.0 × 2.0 cm sections of copper foil aligned parallel to one another and perpendicular to the window and separated from the window by 1 mm and from one another by 1.0 cm. A set of double 2-mm slits (1.0 cm apart, the nearest being 0.5 cm from the outside edge of the cell window) assured that no light fell directly onto the cathode. The electrodes were connected to a Heathkit Model PS4 400 volt power supply and a Keithley Model 153 microvolt-ammeter in series. A bias of 400 V was applied to the electrodes during operation, resulting in a field of 400 V cm^{-1}. The system was tested by inserting a bare 50-V bulb filament between the electrodes. When the cell was evacuated and the filament heated, photoelectron current flow from filament to anode down to the 100-pA region was reproducibly registered.

Photon flux of 300-450-nm light through the slits was about 10^{15} photons s^{-1}. Absorbance by the complex at 0.5 torr over the first two centimeters of pathlength was approximately 1×10^{-2}. At a population of the MLCT state of unity efficiency, the excitation rate would be about 10^{13} molecules s^{-1}, producing a maximum current flow on the order of 10^{13} electrons s^{-1} or about 1 μA. This current is 4 orders of magnitude higher than the limit of detectability for the apparatus.

Solution-Phase Photochemistry. Cyclohexane solutions (4.00 mL) containing 6.75×10^{-3} M $Co(CO)_3NO$ and varying concentrations of entering ligand were prepared by mixing standard solutions of the cobalt complex and the ligand. From each sample solution, 2.70 mL were transferred by volumetric syringe into the irradiation cell. The remainder of the solution served as the thermal blank. All manipulations were performed in a nitrogen atmosphere drybox. All ligand concentrations were expressed in units of [L]/[Co].

Photolysis was carried out by using an optical train consisting of a Hg-Xe 1000-W high-pressure lamp and appropriate filters to isolate the 405- and 436-nm lines. The photon flux, 5×10^{-6} photons s^{-1}, was determined by using potassium ferrioxalate actinometry.[21] Sealed 1-cm Cary cells or 10 cm long Pyrex test tubes containing a ministir bar were used. The cell or tube was capped in the drybox and used throughout the entire irradiation to prevent contamination with atmospheric oxygen. Irradiated solutions and thermal blanks were transferred to infrared cells in air. Irradiation times ranged from 1 to 12 min for solutions containing entering ligands and were 90 min for solutions containing no ligand.

Starting material disappearance and product appearance were monitored by the nitrosyl infrared stretch bands on a Perkin-Elmer 421 infrared spectrophotometer using 0.1-mm sodium chloride cells. Electronic absorption spectra were measured on a Cary 15 UV-visible spectrophotometer. Absorption vs. concentration working curves were constructed to determine the extinction coefficient of the nitrosyl stretch band of $Co(CO)_3NO$. For each absorbance determination the average of six intensity measurements was used. Reproducibility of ±3% was realized by using these techniques.

Each quantum yield was determined twice and the average value reported. The rates of product appearance match those of starting material disappearance within experimental error. All photoreactions were run to 20% or less conversion.

Acknowledgment. The support of the National Science Foundation is gratefully acknowledged. The authors also thank David Ng for preliminary solution-phase photochemical studies.

(32) Young, R. S. "The Analytical Chemistry of Cobalt"; Pergamon Press: New York, 1966; p 443.
(33) Kodama, K. "Methods of Inorganic Analysis", Wiley: New York, 1963; p 443.

Imidazolate- and Oxo-Bridged Metalloporphyrins

John T. Landrum,[1] David Grimmett,[1] Kenneth J. Haller,[2] W. Robert Scheidt,[2] and Christopher A. Reed*[1]

Contribution from the Departments of Chemistry, University of Southern California, Los Angeles, California 90007, and University of Notre Dame, Notre Dame, Indiana 46556.
Received September 12, 1980

Abstract: Urea-linked tetraphenylporphyrin dimers have been synthesized with bridging imidazolate ligands between Fe(II)/Fe(II), Mn(II)/Mn(II), and Mn(II)/Co(II) centers. Magnetic susceptibility measurements down to 4 K show that imidazolate is a relatively weak mediator of antiferromagnetic coupling in these complexes ($-J = 2-5$ cm^{-1}). The heteronuclear Mn(II)/Co(II) dimer, an $S = {}^5/_2/S = {}^1/_2$ spin model for the heme a_3/Cu_B active site of cytochrome oxidase, has $-J = 5$ cm^{-1}. Thus, there is little support for the role of histidyl imidazolate as a bridging ligand between Fe(III) and Cu(II) in cytochrome oxidase where $-J > 200$ cm^{-1}. The magnetic, chemical, and X-ray structural properties of the μ-oxo ferric dimer of the face-to-face porphyrin have been investigated. Crystal data for $[Fe_2(C_{89}H_{56}N_{10}O)]O{\cdot}H_2O{\cdot}2$toluene follow: triclinic, $a = 14.004$ (6) Å, $b = 22.995$ (6) Å, $c = 13.192$ (4) Å, $\alpha = 101.45$ (2)°, $\beta = 93.91$ (2)°, $\gamma = 80.40$ (2)°; space group $P\bar{1}$; $Z = 2$. The average Fe–N distance in the biporphyrin is 2.075 Å, and the average Fe–O distance is 1.787 Å. The iron atoms are displaced 0.60 and 0.65 Å from the mean porphinato planes. The Fe–O–Fe angle is distinctly nonlinear with a value of 161.4°; a water molecule forms a hydrogen-bonding network between the oxo ligand and the hydrogen atoms of the urea link which joins the two halves of the biporphyrin. The two porphinato planes are not coplanar, having a dihedral angle of 15.8°.

The existence of strongly interacting metal sites in bi- and tetranuclear metalloproteins such as hemocyanin, copper oxidases, hemerythrin, superoxide dismutase, and cytochrome oxidase provides an additional impetus for gaining an understanding of the coordination chemistry principles which are unique to multimetal systems.[3] Antiferromagnetic coupling mediated by imidazolate- and oxo-bridging ligands is of particular interest[4-8] as

(1) University of Southern California.
(2) University of Notre Dame.

(3) Cohen, I. A. *Struct. Bonding (Berlin)* **1980**, *40*, 1-37.

0002-7863/81/1503-2640$01.25/0

is the concept of binuclear catalysis.[9] We report herein the synthesis and characterization of some antiferromagnetically coupled face-to-face porphyrin (FF)[10] complexes of iron, manganese, and cobalt. Included is a determination of $-J$ for the first isolated heteronuclear imidazolate-bridged complex which, although containing Mn(II) and Co(II) not Fe(III) and Cu(II), is probably a rather good spin model for cytochrome oxidase, having an $S = {}^5/_2$ high-spin metalloporphyrin interacting with an $S = {}^1/_2$ center.

Experimental Section

Synthesis. General methods and reagents were as previously described.[11]

5-(*o*-Aminophenyl)-10,15,20-triphenylporphyrin (1). Benzaldehyde (61.2 mL), *o*-nitrobenzaldehyde (45.3 g), and pyrrole (62 mL) were heated under reflux in propionic acid (2.5 L) for 25 min. After the solution was allowed to cool, the purple crystalline products (tetraphenylporphyrin, (*o*-nitrophenyl)triphenylporphyrin, and other nitroporphyrins) were collected by filtration and reduced to aminoporphyrins with concentrated HCl (700 mL) and ground stannous chloride (65 g of the dihydrate) at reflux for 30 min. The mixture was carefully neutralized with concentrated ammonium hydroxide, and the porphyrins were extracted into chloroform. Dry-column chromatography on silica gel (8 × 40 cm) with toluene in 4-g batches gave the desired product as the second fraction. Recrystallization from dichloromethane–heptane gave ca. 7 g of purple crystals (~6% based on pyrrole): NMR ($CDCl_3$) δ 7.2 (m,2 H), m, 7.8 (m, 12 H), 8.3 (m, 7 H), 8.98 (3s, 8 H). This synthesis is similar to that reported recently by Collman et al.[12]

***N,N*-Bis(5-(*o*-phenyl)-10,15,20-triphenylporphyrin)urea. Face-to-Face Porphyrin (FF) (2).** (Caution! Phosgene gas is extremely toxic. Use only in a well-drafted hood. As a precaution keep a large open beaker of concentrated ammonia close to possible leaks.) Phosgene was bubbled slowly through a solution of porphyrin **1** (0.5 g) in dry toluene (200 mL) and pyridine (2 mL). Excess phosgene was vented via concentrated ammonia traps. After about 30 min the reaction was checked for completion by TLC and excess phosgene vented by bubbling with nitrogen. The solvent was removed under vacuum, protecting the pump with three liquid nitrogen traps, a long, sodium hydroxide pellet filled tube, and a immediate oil change when completed. To the reaction flask was then added further porphyrin 1 (0.5 g) and dry toluene (200 mL). After the solution was stirred overnight, ammonia (concentrated, aqueous) was added until the green solution remained purple and the solvent volume was reduced on a rotary evaporator. Chromatography on silica gel with toluene gave some unreacted **1** and the desired product (600 mg, 60%). Recrystallization from dichloromethane–heptane and then dichloromethane–methanol was done several times to achieve high purity: IR ν(CO) 1700 (s) cm^{-1}; NMR ($CDCl_3$) δ −2.8 (s, 4 H, pyr NH), 6.9 and 7.5 (m, 2 H, urea NH), 7.8 (m, 24 H, meta and para), 8.3 (m, 14 H, ortho), 9.0 (3s, 8 H, pyr CH). Anal. Calcd for methanol solvate $C_{90}H_{62}N_{10}O_2$: C, 81.01; H, 5.04; N, 10.39. Found: C, 80.61; H, 4.88; N, 10.31.

Fe_2(FF) (3). Method A. Free-base porphyrin **2** (200 mg), $FeBr_2$ (200 mg), and 1,8-bis(dimethylamino)napthalene (Aldrich Proton Sponge) (160 mg) were heated under reflux in THF (50 mL) until the visible spectrum showed the absence of **2** (λ_{max} = 513 nm). Degassed neutral activated alumina (1 g) was added and the solvent carefully evaporated to dryness under vacuum. The product was recovered by chromatography on a short alumina column (8 × 2 cm), eluting with benzene containing 5% ethanol. The product was obtained as an oil by evaporation under vacuum. λ_{max} (THF) at 422, 538, and 600 nm were very similar to those of the well-characterized Fe(TPP).[13]

Fe_2Cl_2(FF)·3CH_2Cl_2 (4). The reaction mixture from above after reflux was air exposed and converted to $Fe_2(\mu$-O)(FF) by chromatography on basic alumina, eluting with dichloromethane. Acidification of the resulting solution with HCl (1 drop, concentrated, aqueous) followed by methanol gave fine purple crystals of the Tris-CH_2Cl_2 solvate: λ_{max} (toluene) 376 sh, 412 (Soret), 508, 576 nm; $\mu_{eff}^{25°C}$ = 5.9 μ_B; $E°$ vs. SCE (Fe(II)/Fe(III)) = −0.35 V. Anal. Calcd for $C_{92}H_{62}N_{10}Fe_2Cl_8O$: C, 64.29; H, 3.64; N, 8.15. Found: C, 64.53; H, 3.71; N, 8.51.

$Fe_2(\mu$-O)(FF)·H_2O·Toluene (5). To a solution of **4** (150 mg) in toluene (50 mL) was added ammonia (0.5 mL, concentrated, aqueous). When the solution was left sitting in a dessicator saturated with heptane vapor, purple crystals were slowly deposited (135 mg, 90%): IR ν(FeO) 845 cm^{-1}, ν(OH) 3350 cm^{-1}; λ_{max} (toluene) 409 (Soret), 573, 610 nm; GLC analysis for toluene calcd 6.1, found 7.2. Anal. Calcd for $C_{96}H_{66}N_{10}Fe_2O_2$: C, 75.89; H, 4.38; N, 9.22. Found: C, 75.71; H, 4.80; N, 9.04.

Fe_2(FF) (3). Method B. A solution of **4** (150 mg) in toluene (50 mL) was stirred over zinc amalgum until complete reduction was indicated spectrally (loss of 509-nm band). The solution was filtered through a fine frit and had a visible spectrum identical with that obtained in method A.

Mn_2(FF) (6). This was prepared by similar methods as above for **3** by using $MnBr_2$ and collected as an oil. λ_{max} (THF) at 412, 432 (Soret), 524, 567, and 607 nm were very similar to those of the well-characterized Mn(TPP).[14]

Mn_2Br_2 (FF)·2CH_2Cl_2 (7). This was prepared in a manner similar to the case for **4** by using HBr in 60% yield: $\mu_{eff}^{24°C}$ = 4.8 μ_B. Anal. Calcd for $C_{91}H_{60}N_{10}Mn_2Cl_4OBr_2$: C, 63.5; H, 3.54; N, 8.14. Found: C, 64.75; H, 4.06; N, 8.03.

[Bu_4N][$Fe_2(\mu$-Im)(FF)]·3THF (8). To a solution of 3 (200 mg) in THF (20 mL) was added 1 equiv of [Bu_4N][Im] (43 mg). The resulting solution was filtered through a medium frit to remove any particulates and set aside to crystallize. Fine purple crystals were collected by filtration and washed with THF: λ_{max} (THF) 402 (sh), 445 (Soret), 530 (sh), 573, 613 nm; GLC solvate analysis for 3THF calcd 11.2, found 10.5. Anal. Calcd for $C_{120}H_{119}N_{13}Fe_2O_4$: C, 75.08; H, 6.25; N, 9.50. Found: C, 74.98; H, 6.52; N, 9.27.

[Bu_4N][$Fe_2(\mu$-2-MeIm)(FF)]·2THF (9). This complex was prepared as above: λ_{max} (THF) 405 (sh), 437 (Soret), 526 (sh), 568, 610 nm. Anal. Calcd for $C_{117}H_{113}N_{14}Fe_2O_3$: C, 74.23; H, 6.08; N, 9.79. Found: C, 73.96; H, 6.11; N, 9.26.

[Bu_4N][$Mn_2(\mu$-Im)(FF)]·2THF (10). This was prepared from Mn_2(FF) in a similar manner to the iron analogue: λ_{max} (THF) 520 (sh), 575, 615 nm. Anal. Calcd for $C_{116}H_{111}N_{13}Mn_2O_3$: C, 75.49; H, 6.50; N, 9.86. Found: C, 75.81; H, 6.53; N, 9.52.

[Bu_4N][MnCo(μ-Im)(FF)]·3THF (11). $MnBr_2$ (700 mg) and aminoporphyrin **1** (600 mg) were heated under reflux in THF (100 mL) until visible spectroscopy indicated the reaction was complete. Upon exposure to air and after the solvent was stripped on a rotary evaporator, the product was obtained by chromatography on silica gel, eluting first with toluene and then with toluene–acetone (5%). Recrystallization from CH_2Cl_2–heptane gave purple crystals of product presumed to be MnBr(*o*-NH_2TPP) (450 mg). Phosgene was slowly bubbled through a dry toluene (90 mL) solution of aminoporphyrin **1** (450 mg) followed by evacuation as in the preparation of **2**. The resulting isocyanate was redissolved in toluene (140 mL), and after addition of the MnBr(*o*-NH_2TPP) prepared above the mixture was stirred overnight. Chromatography on silica gel with CH_2Cl_2 followed by CH_2Cl_2–acetone (5%) gave successively **1**, **2**, the desired monometalated MnBr(FF), and finally some unreacted MnBr(*o*-NH_2TPP). Recrystallization from CH_2Cl_2–heptane gave purple crystals of MnBr(FF)·2CH_2Cl_2 (150 mg): λ_{max} (toluene) 413 (Soret), 478 (Soret), 528, 567, 606 nm. Anal. Calcd for $C_{91}H_{62}N_{10}OMnBrCl_4$: C, 68.82; H, 3.93; N, 8.82. Found: C, 68.77; H, 4.22; N, 8.75. This material was treated with excess $Co(OAc)_2$ in $CHCl_3$ under reflux until metallation was complete. Chromatography on silica gel with CH_2Cl_2–acetone (5%) followed by recrystallization from CH_2Cl_2–heptane gave purple crystals of product presumed to be MnBrCo(FF): λ_{max} (toluene) 412, 478, 528, 578, 612; ($CHCl_3$) 412, 473, 528, 573, 610 nm. This product was reduced in THF by stirring over zinc amalgum using the Soret maximum of Mn(II) (438 nm) to follow the reaction. Recrystallization from toluene–heptane gave a purple

(4) Palmer, G.; Babcock, G. T.; Vickery, L. E. *Proc. Natl. Acad. Sci. U.S.A.* **1976**, *73*, 2206–2210.
(5) Landrum, J. T.; Reed, C. A.; Hatano, K.; Scheidt, W. R. *Proc. Natl. Acad. Sci. U.S.A.* **1978**, *101*, 3232–3234.
(6) O'Young, C.-L.; Dewan, J. C.; Lilienthal, H. R.; Lippard, S. J. *J. Am. Chem. Soc.* **1978**, *100*, 7291–7300.
(7) Reed, C. A.; Landrum, J. T. *FEBS Lett.* **1979**, *106*, 265–267.
(8) Petty, R. H.; Welch, B. R.; Wilson, K. J.; Bottomley, L. A.; Kadish, K. M. *J. Am. Chem. Soc.* **1980**, *102*, 611–620.
(9) Collman, J. P.; Denisevich, P.; Konai, Y.; Morrocco, M.; Koval, C.; Anson, F. *J. Am. Chem. Soc.* **1980**, *102*, 6027–6036.
(10) Abbreviations used in this paper: Im, imidazolate, FF, dianion of face-to-face porphyrin (see Scheme I); THF, tetrahydrofuran; Bu_4NIm, tetra-*n*-butylammonium imidazolate; DMF, dimethylformamide; TPP, dianion of tetraphenylporphyrin; $ProtoMe_2$, dianion of the dimethyl ester of protoporphyrin IX; ODM, dianion of 5,15-dimethyloctaethylporphyrin; salen, *N,N'*-ethylenebis(salicylaldiminato) anion.
(11) Landrum, J. T.; Hatano, K.; Scheidt, W. R.; Reed, C. A. *J. Am. Chem. Soc.* **1980**, *102*, 6027–6036.
(12) Collman, J. P.; Brauman, J. I.; Doxsee, K. M.; Halbert, T. R.; Bunnenberg, E.; Linder, R. E.; LaMar, G. N.; Del Gaudio, J.; Lang, G.; Spartalian, K. *J. Am. Chem. Soc.* **1979**, *101*, 2948–2958.
(13) Collman, J. P.; Hoard, J. L.; Kim, N.; Lang, G.; Reed, C. A. *J. Am. Chem. Soc.* **1975**, *97*, 2676–2681.
(14) Reed, C. A.; Kouba, J. K.; Grimes, C. J.; Cheung, S. K. *Inorg. Chem.* **1978**, *17*, 2666–2670.

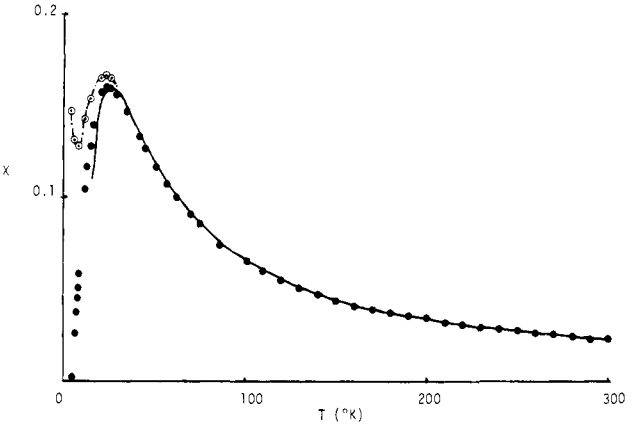

Figure 1. Plot of χ_M (cgs unit) vs. temperature for the Fe(II)/Fe(II) complex **8** corrected for diamagnetism only (open circles, ···). The solid circles are data points corrected for both diamagnetism and paramagnetic impurities. The solid line is the calculated fit for $-J = 2.3$ cm^{-1}, $g = 2.15$, and $\Theta = 13$ K.

powder presumed to be CoMn(FF). This product (137 mg) was treated with [Bu_4N][Im] (30 mg) in THF (9 mL) and the solution filtered through a medium frit. Upon evaporation to dryness under vacuum, being redissolved in THF (2 mL), and being left to stand, purple crystals of the final product were deposited: λ_{max} (DMF) 412, 436, 528, 572, 616 nm. Anal. Calcd for $C_{120}H_{119}N_{13}CoMnO_4$: C, 74.96; H, 6.20; N, 9.47. Found: C, 74.01; H, 6.29; N, 9.11.

Magnetic Susceptibility Measurements and Results. All data were collected on an automated Faraday system at Bell Labs by courtesy of Frank DiSalvo except those for the dimanganese imidazolate complex **10** which were recorded on an SCT squid system at Stanford University by courtesy of J. P. Collman. Raw data were corrected for diamagnetism ($\chi_M^{DIA} = 1.4 \times 10^{-3}$ cgs unit) and for paramagnetic impurities in two ways. For the μ-oxo complex **5** extrapolation of the low-temperature $1/\chi_M$ vs. T data to high temperature allows simple substraction at all temperatures since **5** should be diamagnetic at very low temperatures. This correction was equivalent to 2.5% high-spin Fe(III). For the diiron imidazolate complexes **8** and **9** the method of Ginsberg[15] was used. These corrections were equivalent to approximately 7% and 10% high-spin Fe(III), respectively, the most likely impurity. For complex **10** a good estimate of the correction was not possible. In the case of the manganese–cobalt mixed-metal imidazolate species, **11**, no correction for paramagnetic impurities was applied because we know of no legitimate procedure for cases such as this which do not approach diamagnetism at liquid-helium temperatures. Final data are tabulated as supplementary material (Table I). These were fitted to the standard theory[16] on the basis of $H = -2JS_1S_2$ by visual comparison to curves generated by a computer. Systematic variation of the variables g, J, and θ led rapidly to the reported fits. The $S = 2$ state for Fe(II), the $S = {}^5/_2$ state for Mn(II) and the $S = {}^1/_2$ state for Co(II) can be safely assumed from the room-temperature magnetic moments and the spectral similarity of these species to their isostructural imidazole analogues Fe(2-MeImH)(TPP),[17] Mn(1-MeIm)(TPP),[14] and Co(1-MeIm)(TPP).[18] An estimate of g, the gyromagnetic ratio, was obtained by using eq 1, where Θ is the Weiss

$$\mu_{eff}^2 = g^2S(S+1) + (g^2S(S+1)\Theta/T) \quad (1)$$

constant. At high temperatures $\Theta/T \ll 1$ so the second term can be neglected. In the case of the iron complexes **8** and **9** Weiss constants of 13 and 8 K had to be included such that T was replaced by $T-\theta$ in the theoretical equation. This takes into account interactions between molecules otherwise assumd to be zero. Graphically θ has the effect of shifting the χ_M curve to higher temperatures. Best fits are plotted along with corrected data points in Figures 1–5 by using cgs units, and the final values of g, J, and θ are given in the figure captions. Uncorrected data for **8** are also shown in Figure 1 to illustrate the effect of paramagnetic impurities.

X-ray Structure Determination. Preliminary examination of a single-crystal of $Fe_2(\mu\text{-}O)(FF)\cdot H_2O\cdot 2$toluene on a Syntex P$\bar{1}$ diffractometer indicated a two-molecule triclinic unit cell, space group $P1$ or $P\bar{1}$. A Delauney reduction did not indicate any hidden symmetry. Precise lattice

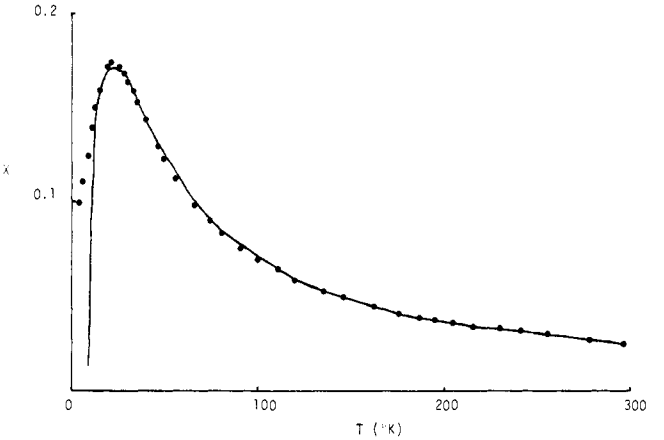

Figure 2. Plot of χ_M (cgs unit) vs. temperature for the Fe(II)/Fe(II) 2-methylimidazolate complex **9**. The curve is the calculated fit with $-J = 2.35$ cm^{-1}, $g = 2.25$, and $\Theta = 8$ K.

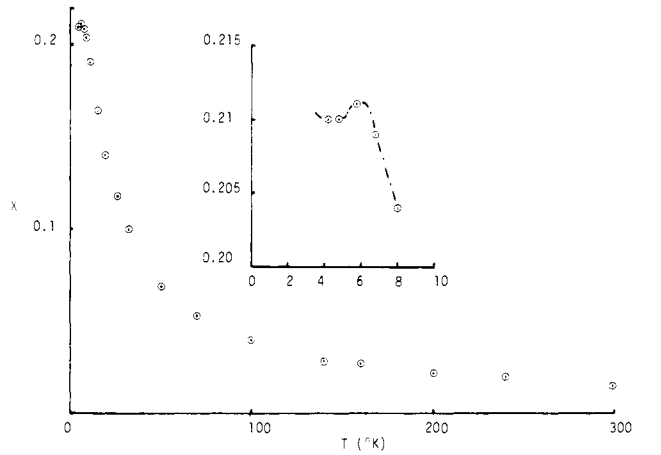

Figure 3. Plot of χ_M (cgs unit) vs. temperature for the Mn(II)/Mn(II) complex **10**. No calculated fit was attempted because an accurate estimate of paramagnetic impurities (see insert) could not be made. The position of T_{max} puts $-J \simeq 2$ cm^{-1}.[16]

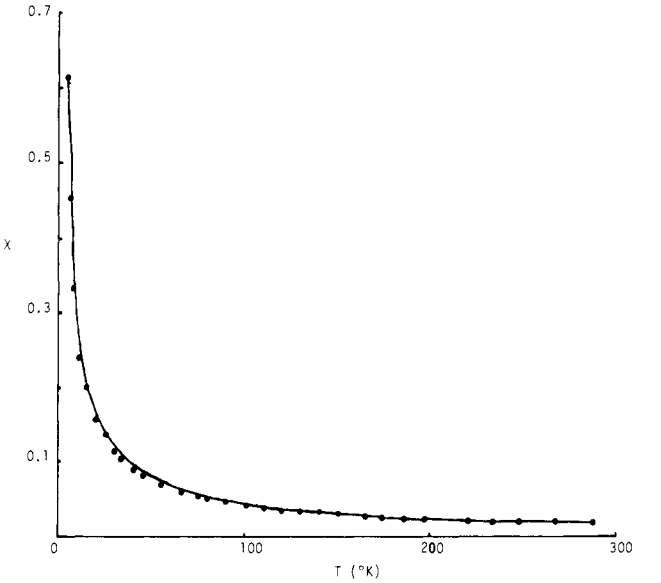

Figure 4. Plot of total χ (cgs unit) vs. temperature for the Mn(II)/Co(II) complex **11**, corrected for diamagnetism only. The curve is a calculated fit for $-J = 5$ cm^{-1} and $g = 2.0$.

constants were obtained from the setting angles of 60 reflections measured at $\pm 2\theta$ and led to the cell constants reported in Table II.

Intensity data were measured on a Syntex P$\bar{1}$ diffractometer; a summary of the intensity collection values are given in Table II. Four

(15) Ginsberg, A. P. *Inorg. Chim. Acta Rev.* **1971**, *4*, 45–68.
(16) Wojciechowski, W. *Inorg. Chim. Acta* **1967**, *1*, 319–334.
(17) Collman, J. P.; Reed, C. A. *J. Am. Chem. Soc.* **1973**, *95*, 2048–2049.
(18) Scheidt, W. R. *J. Am. Chem. Soc.* **1974**, *96*, 90–94.

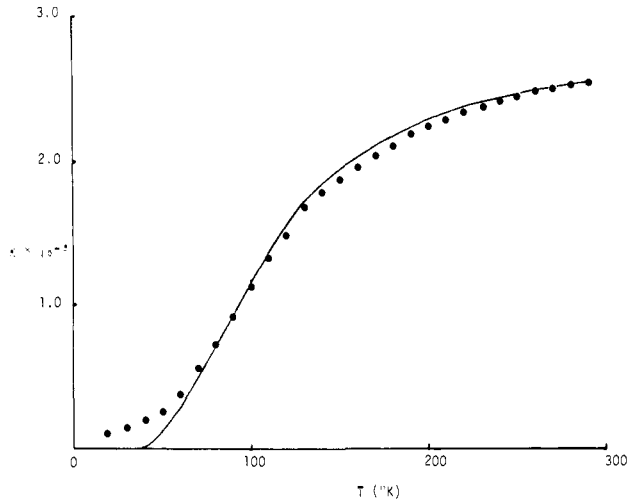

Figure 5. Plot of χ_M (cgs unit) vs. temperature for the μ-oxo complex **5**. The curve is a calculated fit for $-J = 107.5$ cm^{-1} and $g = 2.0$, assuming the high-spin $S = {}^5/_2$ ferric state for each iron atom.

Table II. Summary of Crystal Data and Intensity Data Collection Parameters for $Fe_2(\mu\text{-O})FF\cdot H_2O\cdot 2$Toluene

temp, °C	20 ± 1 °C
cryst dimens, mm	0.09 × 0.20 × 0.55
space group	$P\bar{1}$ (No. 2)
Z	2
unit cell a, Å	14.004 (6)
b, Å	22.995 (6)
c, Å	13.192 (4)
α, deg	101.45 (2)
β, deg	93.91 (2)
γ, deg	80.40 (2)
vol, Å^3	4102.8
calcd density, g/cm^3	1.30
obsd density, g/cm^3	1.295
radiatn	graphite-monochromated Mo Kα ($\bar{\lambda} = 0.710\,73$ Å)
μ, mm^{-1}	0.370
scan method	wandering ω
scan range	0.18° centered on K$\bar{\alpha}$
bkgd	0.85° on either side of the peak, each for 0.25 times the total scan time
$(\sin\theta)/\lambda$, Å^{-1}	0.602
criterion for obsd	$F_o > 3\sigma(F_o)$
unique obsd data	7478

standard reflections were measured every 50 reflections during data collection to monitor the long-term stability; no significant trends were observed. All independent data for $(\sin\theta)/\lambda \leq 0.602$ Å^{-1} were measured. Intensity data were reduced and standard deviations calculated as described previously.[19] An empirical absorption correction[20] was applied to the data. A total of 7478 reflections had $F_o > 3\sigma(F_o)$ and were used in all subsequent calculations.

The space group $P\bar{1}$ was assumed for the structural analysis. The structure was solved by the heavy-atom method.[21] A series of difference Fourier calculations readily gave positions for the atoms of the biporphyrin, the oxo ligand, the water molecule, and one toluene molecule of crystallization. The water molecule was subsequently discovered to take a major and minor position which are chemically indistinguishable and with final refined occupancies of 0.72 (2) and 0.14 (2). The position of the second toluene molecule of crystallization proved to be quite troublesome. Difference Fourier maps indicated a region of diffuse electron density, substantially larger than needed to accommodate an ordered toluene molecule. This region was modeled, albeit not in a completely satisfactory manner, with three rigid toluene groups of varying occupancies.

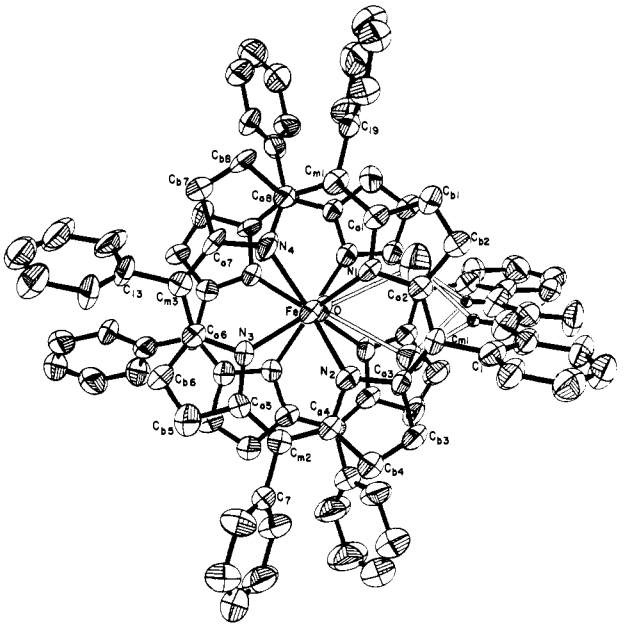

Figure 6. An ORTEP plot of the $Fe_2(\mu\text{-O})(FF)\cdot H_2O$ molecule. The 1Fe···2Fe axis is perpendicular to the plane of the paper. The atom-labeling scheme is displayed for the upper porphinato core; in the tables the labels are preceeded by the prefix 1. The labels used for the lower core are identical and preceeded by the number 2 and can be recognized from this figure by rotating the labels counterclockwise ~20°. The water molecule involved in the hydrogen bonding is displayed; the hydrogen bonds are shown as open bonds. For clarity, hydrogen atoms, except for the two hydrogen atoms of the urea link, have not been drawn. Probability ellipsoids are drawn at the 50% level.

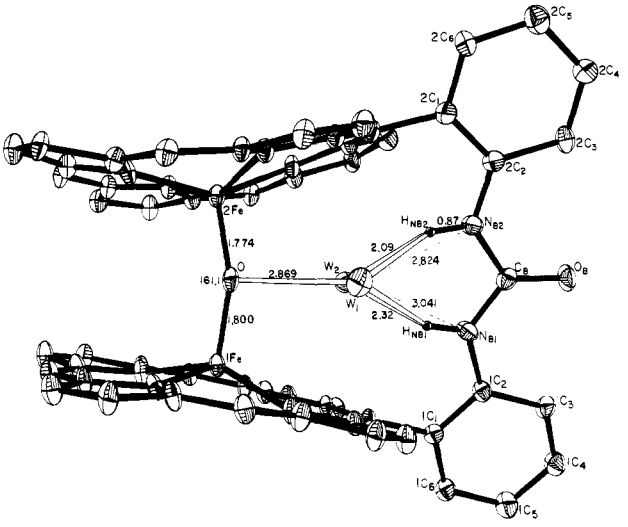

Figure 7. A second view of the $Fe_2(\mu\text{-O})(FF)\cdot H_2O$ molecule. The atom labels used for the urea bridge are displayed as well as separations involving water (W_1). The remaining six phenyl groups have been eliminated for clarity.

The structural model was refined by block-diagonal and full-matrix least-squares methods.[22] The final model has 1205 variables and was segmented into five blocks for the full-matrix refinement. Although some hydrogen atoms positions were found in difference maps, only the two hydrogen atoms of the urea linkage that are involved in hydrogen bonding to the water were included in the refinement. Final least-squares refinement led to $R_1 = \sum(|F_o| - |F_c|)^2/\sum(F_o)$ of 0.115 and $R_2 = \sum[w(|F_o| - |F_c|)^2/\sum w(F_o)^2]^{1/2}$ of 0.120, an error of fit of 2.84 and a final data to

(19) Scheidt, W. R. *J. Am. Chem. Soc.* **1974**, *96*, 84–90.
(20) North, A. C. T.; Phillips, D. C.; Matthews, F. S. *Acta Crystallogr., Sect. A* **1968**, *A24*, 351–359.
(21) A locally modified version of the Fourier program ALFF was used: Hubbard, C. R.; Quicksall, C. O.; Jacobsen, R. A. Report IS-2625, Ames Laboratory; Iowa State University: Ames, Iowa, 1971.
(22) Locally modified versions of REFINE by J. J. Park and ORFLS by Busing, Levy, and Martin were used. Atomic form factors from: Cromer, D. T.; Mann, J. B. *Acta Crystallogr., Sect. A* **1968**, *A24*, 321–324 (with real and imaginary corrections for anomalous scattering in the form factor of the iron atoms from: Cromer, D. T.; Liberman, D. *J. Chem. Phys.* **1970**, *53*, 1891–1898.

Table III. Fractional Triclinic Coordinates for $Fe_2(\mu\text{-}O)FF\cdot H_2O$

atom	x	y	z	atom	x	y	z
1Fe	0.26061 (9)	0.19768 (6)	0.18934 (11)	$2N_4$	0.3501 (5)	0.3436 (3)	0.4328 (6)
$1N_1$	0.1815 (5)	0.2151 (3)	0.0596 (6)	$2C_{a8}$	0.3768 (6)	0.3874 (4)	0.3874 (7)
$1N_2$	0.1725 (5)	0.1320 (3)	0.1905 (6)	$2C_{a7}$	0.4312 (6)	0.3244 (4)	0.4918 (7)
$1N_3$	0.3658 (5)	0.1435 (3)	0.2585 (6)	$2C_{a6}$	0.3590 (6)	0.2499 (4)	0.5594 (7)
$1N_4$	0.3723 (5)	0.2286 (3)	0.1301 (6)	$2C_{a5}$	0.2148 (7)	0.2229 (4)	0.5523 (7)
$1C_{a1}$	0.1924 (7)	0.2584 (4)	0.0035 (8)	$2C_{a4}$	0.0519 (7)	0.2720 (4)	0.5057 (7)
$1C_{a2}$	0.880 (6)	0.2023 (4)	0.0277 (7)	$2C_{a3}$	−0.0049 (6)	0.3531 (4)	0.4382 (7)
$1C_{a3}$	0.0800 (6)	0.1303 (4)	0.1416 (7)	$2C_{a2}$	0.0652 (6)	0.4170 (4)	0.3456 (7)
$1C_{a4}$	0.1846 (6)	0.0906 (4)	0.2535 (7)	$2C_{a1}$	0.2149 (6)	0.4269 (4)	0.3178 (7)
$1C_{a5}$	0.3525 (6)	0.1016 (4)	0.3157 (8)	$2C_{b8}$	0.4763 (7)	0.3949 (5)	0.4178 (8)
$1C_{a6}$	0.4637 (7)	0.1502 (4)	0.2799 (8)	$2C_{b7}$	0.5072 (7)	0.3566 (5)	0.4857 (8)
$1C_{a7}$	0.4690 (7)	0.2241 (5)	0.1646 (8)	$2C_{b6}$	0.3669 (7)	0.1977 (4)	0.6104 (8)
$1C_{a8}$	0.3623 (6)	0.2691 (4)	0.0644 (8)	$2C_{b5}$	0.2772 (7)	0.1815 (5)	0.6050 (8)
$1C_{b1}$	0.1077 (7)	0.2724 (5)	−0.0646 (8)	$2C_{b4}$	−0.0547 (7)	0.2833 (5)	0.5143 (8)
$1C_{b2}$	0.0445 (7)	0.2373 (5)	−0.0490 (8)	$2C_{b3}$	−0.0899 (7)	0.3352 (5)	0.4757 (9)
$1C_{b3}$	0.0380 (6)	0.0856 (4)	0.1771 (8)	$2C_{b2}$	0.0559 (7)	0.4630 (4)	0.2852 (8)
$1C_{b4}$	0.1010 (7)	0.0611 (4)	0.2453 (8)	$2C_{b1}$	0.1490 (7)	0.4688 (4)	0.2645 (8)
$1C_{b5}$	0.4391 (8)	0.0859 (5)	0.3783 (9)	$2C_{m1}$	−0.0111 (6)	0.3987 (4)	0.3832 (7)
$1C_{b6}$	0.5059 (7)	0.1163 (5)	0.3560 (9)	$2C_{m2}$	0.1115 (7)	0.2267 (4)	0.5422 (7)
$1C_{b7}$	0.5191 (7)	0.2608 (5)	0.1168 (8)	$2C_{m3}$	0.4353 (6)	0.2795 (4)	0.5493 (8)
$1C_{b8}$	0.4525 (7)	0.2890 (5)	0.0556 (8)	$2C_{m4}$	0.3168 (7)	0.4242 (4)	0.3293 (7)
$1C_{m1}$	0.0410 (6)	0.1627 (4)	0.0679 (7)	$2C_1$	−0.1141 (7)	0.4276 (4)	0.3610 (8)
$1C_{m2}$	0.2668 (7)	0.0766 (4)	0.3141 (7)	$2C_2$	−0.1747 (7)	0.3986 (4)	0.2886 (7)
$1C_{m3}$	0.5116 (7)	0.1864 (4)	0.2337 (8)	$2C_3$	−0.2771 (7)	0.4250 (5)	0.2787 (8)
$1C_{m4}$	0.2777 (7)	0.2844 (4)	0.0054 (8)	$2C_4$	−0.3090 (7)	0.4810 (5)	0.3379 (8)
$1C_1$	−0.0597 (7)	0.1554 (4)	0.0251 (7)	$2C_5$	−0.2462 (9)	0.5130 (5)	0.4095 (9)
$1C_2$	−0.1358 (7)	0.2026 (4)	0.0495 (7)	$2C_6$	−0.1459 (7)	0.4852 (5)	0.4180 (8)
$1C_3$	−0.2316 (7)	0.1957 (5)	0.0044 (8)	$2C_7$	0.0641 (7)	0.1807 (5)	0.5769 (9)
$1C_4$	−0.2430 (7)	0.1432 (5)	−0.0631 (9)	$2C_8$	0.0654 (9)	0.1775 (6)	0.6816 (10)
$1C_5$	−0.1670 (8)	0.0951 (5)	−0.0874 (9)	$2C_9$	0.0154 (12)	0.1341 (7)	0.7111 (12)
$1C_6$	−0.0723 (7)	0.1030 (5)	−0.0424 (8)	$2C_{10}$	−0.0349 (10)	0.0985 (7)	0.6359 (14)
$1C_7$	0.2723 (7)	0.0254 (5)	0.3706 (9)	$2C_{11}$	−0.0338 (9)	0.1013 (6)	0.5326 (12)
$1C_8$	0.2264 (8)	0.0368 (5)	0.4670 (10)	$2C_{12}$	0.0187 (8)	0.1431 (5)	0.5011 (9)
$1C_9$	0.2325 (10)	−0.0124 (7)	0.5208 (11)	$2C_{13}$	0.5280 (7)	0.2646 (4)	0.6100 (8)
$1C_{10}$	0.2827 (9)	−0.0701 (7)	0.4751 (13)	$2C_{14}$	0.5264 (8)	0.2753 (5)	0.7175 (9)
$1C_{11}$	0.3260 (10)	−0.0783 (6)	0.3846 (13)	$2C_{15}$	0.6157 (10)	0.2619 (6)	0.7744 (10)
$1C_{12}$	0.3203 (9)	−0.0308 (5)	0.3314 (10)	$2C_{16}$	0.7012 (9)	0.2384 (6)	0.7223 (13)
$1C_{13}$	0.6195 (7)	0.1849 (6)	0.2562 (9)	$2C_{17}$	0.7007 (8)	0.2282 (5)	0.6175 (11)
$1C_{14}$	0.6544 (8)	0.2380 (6)	0.3046 (9)	$2C_{18}$	0.6130 (7)	0.2407 (5)	0.5574 (9)
$1C_{15}$	0.7568 (10)	0.2326 (8)	0.3270 (10)	$2C_{19}$	0.3637 (8)	0.4658 (5)	0.2797 (9)
$1C_{16}$	0.8158 (10)	0.1753 (10)	0.3013 (13)	$2C_{20}$	0.3388 (8)	0.5277 (5)	0.3134 (9)
$1C_{17}$	0.7792 (10)	0.1254 (9)	0.2576 (13)	$2C_{21}$	0.3825 (10)	0.5684 (6)	0.2665 (13)
$1C_{18}$	0.6761 (8)	0.1279 (6)	0.2329 (9)	$2C_{22}$	0.4510 (12)	0.5434 (8)	0.1944 (13)
$1C_{19}$	0.2757 (6)	0.3342 (5)	−0.0536 (9)	$2C_{23}$	0.4759 (9)	0.4814 (7)	0.1600 (10)
$1C_{20}$	0.2745 (7)	0.3920 (5)	0.0070 (9)	$2C_{24}$	0.4345 (8)	0.4401 (6)	0.2043 (9)
$1C_{21}$	0.2759 (9)	0.4413 (6)	−0.0425 (14)	O	0.2194 (4)	0.25989 (27)	0.2907 (5)
$1C_{22}$	0.2782 (10)	0.4290 (8)	−0.1540 (16)	N_{B1}	−0.1187 (5)	0.2541 (4)	0.1213 (6)
$1C_{23}$	0.2787 (9)	0.3711 (8)	−0.2110 (11)	N_{B2}	−0.1367 (5)	0.3438 (4)	0.2323 (6)
$1C_{24}$	0.2769 (8)	0.3218 (6)	−0.1611 (10)	C_B	−0.1815 (8)	0.3041 (4)	0.1599 (8)
2Fe	0.21662 (9)	0.31299 (6)	0.40854 (11)	O_B	−0.2701 (5)	0.3120 (3)	0.1360 (6)
$2N_1$	0.1623 (5)	0.3953 (3)	0.3663 (6)	W_1	0.0593 (8)	0.3153 (5)	0.1774 (9)
$2N_2$	0.0779 (5)	0.3164 (3)	0.4576 (6)	W_2	0.027 (3)	0.2389 (19)	0.281 (3)
$2N_3$	0.2647 (5)	0.2634 (3)	0.5226 (6)				

[a] The estimated standard deviations of the least significant digits are given in parentheses.

parameter ratio of 6.2. The relatively high R values are the result, at least in part, of the difficulties associated with the disordered toluene solvate. A final difference Fourier had several peaks ranging up to 0.8 e/Å^3 associated with the iron atoms and the bridging oxygen atom. A final listing of the observed and calculated structure factor amplitudes is available as supplementary material.

Final atomic coordinates and the associated anisotropic temperature factors are given in Tables III and IV, respectively. Table V, the root-mean-square displacements of the atoms, is available as supplementary material. Final group parameters and derived atomic coordinates for the toluene molecules are given in Table VIII of the supplementary material.

Description of the $Fe_2(\mu\text{-}O)(FF)\cdot H_2O$ Structure. Two perspective views of the molecule are given in Figures 6 and 7. Figure 6 is a view down the Fe···Fe axis; Figure 7 is a view perpendicular to the plane defined by the Fe···Fe vector and the vector joining the bridging oxo ligand and the oxygen atom of the urea link. Figures 6 and 7 present the atom-labeling scheme as explained in the captions to the two figures. As can be seen from Figure 7, the two porphinato planes of the biporphyrin are not coplanar but form a dihedral angle of 15.8°. Perpendicular separations between atoms of one porphinato core to the mean plane of the other core range from 3.57 to 5.71 Å. The closest interatomic distance between atoms of the two cores is 3.95 Å. Figure 7 also clearly shows the distinctly nonlinear Fe–O–Fe moiety; the value of the angle is 161.1 (4)°.

Individual values for the bond distances and angles of the molecule are displayed in Tables VI and VII, respectively. The geometry of the two FeN_4O coordination groups is generally typical of five-coordinate high-spin iron(III)–porphinato derivatives; the averaged Fe–N distance is 2.075 (19) Å and the average Fe–O distance is 1.787 (18) Å. Additional averaged values for chemically equivalent bond distances and bond angles are shown on the formal diagram of the porphinato core in Figure 8. The numbers in parentheses are the estimated standard deviations calculated on the assumption that all values are drawn from the same population.

Figure 8 also displays the perpendicular displacements, in units of 0.01 Å, of the individual atoms from the mean plane of their respective cores. N_1 of both cores is at the upper right of the diagram, N_2 at the lower right, and so forth. The displacements of the atoms of core 1 are the upper value of the pair of values; the corresponding displacement for core 2 is the lower value. A positive value represents a displacement toward the center of the molecule toward the bridging oxo ligand. An examination of Figure 8 shows that porphinato core 1 displays relatively small

Scheme I. Synthetic Scheme for the Urea-linked Face-to-Face Porphyrin (FF) and Its Imidazolate Complexes

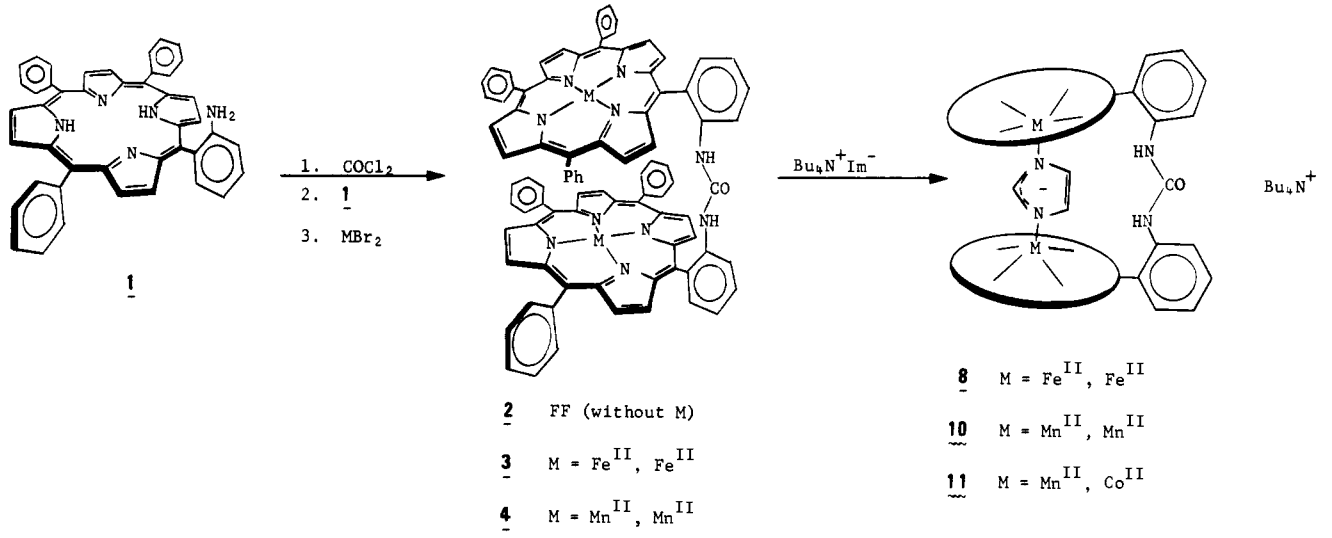

1

2 FF (without M)

3 M = Fe^{II}, Fe^{II}

4 M = Mn^{II}, Mn^{II}

8 M = Fe^{II}, Fe^{II}

10 M = Mn^{II}, Mn^{II}

11 M = Mn^{II}, Co^{II}

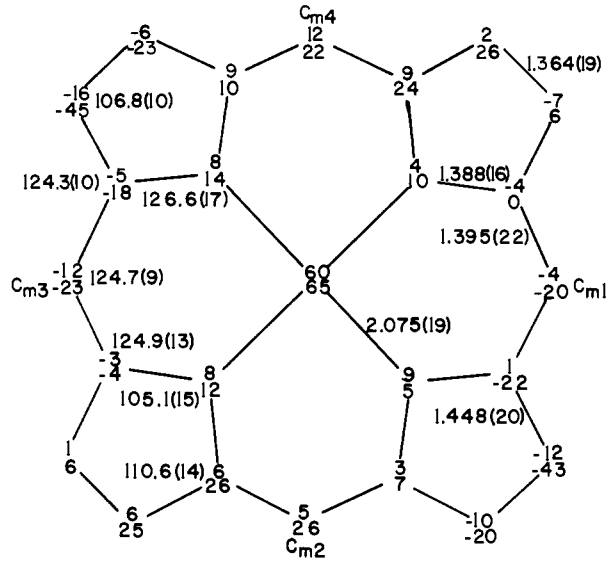

Figure 8. A formal diagram of a porphinato core displaying the perpendicular displacements of the atoms, in units of 0.01 Å, from the mean place of the respective 24-atom cores. The diagram has the same approximate orientation as the cores in Figure 7. The upper value of each pair of values refers to the core carrying the prefix 1 and the lower the prefix 2. The figure also displays the averaged values for the chemically equivalent bond distances and angles in the two halves of the molecule. The number in parentheses following each averaged value is the estimated standard deviation calculated on the assumption that the values are drawn from the same population.

displacements from planarity while core 2 exhibits a substantial S_4 ruffling. The iron atom displacements of 0.60 and 0.65 Å (1Fe and 2Fe respectively) are slightly larger than normal for high-spin five-coordinate iron(III) porphyrins. The iron atom displacements from the respective mean planes of the four nitrogen atoms decrease to 0.52 and 0.55 Å, respectively for 1Fe and 2Fe. The two cores thus display a slightly larger amount of doming or separation (0.08 and 0.10 Å) between the 24-atom core and the four nitrogen atom mean plane than is normal.

The four-atom urea group is planar and the entire bridging unit comprised of the two phenyl groups, and the urea is almost planar with a dihedral angle between the two phenyl groups of 4.6°. The bridging group is not perpendicular to the two cores but rather forms dihedral angles of 70.9 and 70.6°, with cores 1 and 2, respectively. This allows the two cores to become somewhat staggered with respect to each other (see Figure 6) rather than a sterically unfavorable eclipsed conformation. The observed angle of twist, as measured by the 1N–1Fe–2Fe–2N dihedral angles is approximately 24°, to be compared to the 45° value for a completely staggered conformation. Dihedral angles between the other phenyl groups and the respective mean planes range between 59 and 77°. A survey of intermolecular separations appears reasonable with observed distances ranging upward from 3.2 Å.

Discussion

Synthesis. The synthetic strategy behind the urea-linked face-to-face porphyrin (FF) (see Scheme I) was to produce an entropically favored coordination site for a bridging imidazolate ligand. With use of a biporphyrin with a single linkage, rather than the original face-to-face porphyrins with symmetrical double linkages,[23] rotational flexibility is guaranteed while retaining the latent entropic effect to sequester imidazolate and other bridging ligands. This flexibility and lack of high symmetry is crucial to providing workable solubility as evidenced by the extremely high toluene solubility of the unbridged Fe_2(FF) compared to say Fe(TPP). Indirect evidence for rotational flexibility comes from aerobic oxidation of Fe_2(FF) which, by TLC, shows two major μ-oxo products which can be easily equilibrated to a single compound with water or base. Presumably, both the symmetrical intramolecular face-to-face μ-oxo dimer is formed along with intermolecular dimers or oligomers which may have their porphyrin planes oriented exo or endo to each other. Upon equilibration with water, hydrolytic substitution of the oxo bridge together with rotation of the urea linkage must allow total domination of the most thermodynamically stable form. By X-ray crystallography this is shown to be the discrete monomer (of the biporphyrin) having an endo or face-to-face configuration of its porphyrin planes. This is the sole species formed when $Fe_2(\mu$-O)(FF) is prepared by aqueous base treatment of Fe_2Cl_2(FF).

Treatment of the soluble four-coordinate complexes Fe_2(FF), Mn_2(FF), and MnCo(FF) with 1 equiv of tetra-*n*-butylammonium imidazolate, a convenient source of the anion,[11] causes the respective imidazolate salts **8**, **10**, and **11** to crystallize directly out of THF. Their low solubility, which effectively prevents recrystallization, is consistent with the rigid symmetrical face-to-face structures assigned to them in Scheme I. The visible spectra are also consistent with their proposed structures since their λ_{max} values, and spectral shapes are closely related to their five-coordinate imidazole counterparts Fe(2-MeImH)(TPP)[17] and Mn(1-MeIm)(TPP).[14] Expectedly,[11] the Soret maxima of the anionic imidazolates are red-shifted relative to the neutral imidazole species. The observation of antiferromagnetic coupling also provides circumstantial evidence for the correct structural assignments, and we are unable to envisage any reasonable alternatives that fit the molecular formula. Unfortunately, we have as yet been unable to grow crystals of any imidazolate derivative large enough for single-crystal X-ray analysis despite the relatively slow deposition. The dicobalt species $[Co_2(Im)(FF)]^-$ was syn-

(23) Collman, J. P.; Eliot, C. M.; Halbert, T. R.[Tovrog, B. S. *Proc. Natl. Acad. Sci. U.S.A.* **1977**, *74*, 18–22.

Table IV. Anisotropic Thermal Parameters for $Fe_2(\mu\text{-}O)FF\cdot H_2O$

atom	B_{11}	B_{22}	B_{33}	B_{12}	B_{13}	B_{23}
1Fe	2.42 (6)	4.53 (7)	5.26 (8)	−1.17 (5)	0.17 (5)	1.78 (6)
$1N_1$	2.6 (4)	5.0 (4)	6.0 (4)	−1.8 (3)	−0.2 (3)	2.6 (4)
$1N_2$	3.1 (4)	4.1 (4)	6.1 (5)	−1.3 (3)	−0.1 (3)	1.9 (3)
$1N_3$	2.1 (4)	5.3 (4)	6.4 (5)	−0.4 (3)	−0.3 (3)	2.9 (4)
$1N_4$	2.1 (4)	5.5 (4)	7.0 (5)	−0.5 (3)	1.1 (3)	1.4 (4)
$1C_{a1}$	3.9 (5)	6.3 (6)	6.3 (6)	−2.4 (5)	−0.7 (4)	3.0 (5)
$1C_{a2}$	3.0 (5)	5.2 (5)	5.0 (5)	−0.9 (4)	0.2 (4)	2.3 (4)
$1C_{a3}$	2.1 (4)	5.6 (5)	5.6 (5)	−1.0 (4)	−0.4 (4)	1.4 (4)
$1C_{a4}$	2.7 (5)	4.9 (5)	5.7 (6)	−1.3 (4)	−0.1 (4)	2.3 (4)
$1C_{a5}$	3.1 (5)	5.5 (5)	6.3 (6)	−0.8 (4)	−0.8 (4)	3.3 (5)
$1C_{a6}$	3.1 (5)	5.3 (6)	7.9 (7)	−0.7 (4)	0.5 (5)	3.5 (5)
$1C_{a7}$	2.1 (5)	7.1 (6)	7.2 (6)	−2.0 (4)	0.5 (4)	2.8 (5)
$1C_{a8}$	2.5 (5)	4.9 (5)	7.0 (6)	−0.4 (4)	0.4 (4)	3.4 (5)
$1C_{b1}$	3.3 (5)	7.8 (7)	6.2 (6)	−2.1 (5)	−0.7 (5)	2.9 (5)
$1C_{b2}$	3.8 (5)	7.1 (6)	5.6 (6)	−1.4 (5)	0.1 (4)	3.3 (5)
$1C_{b3}$	2.9 (5)	4.7 (5)	6.1 (6)	−1.4 (4)	0.5 (4)	1.8 (4)
$1C_{b4}$	3.3 (5)	5.6 (6)	7.0 (6)	−1.0 (4)	0.3 (5)	2.8 (5)
$1C_{b5}$	4.4 (6)	7.6 (7)	7.1 (7)	−1.5 (5)	−1.1 (5)	2.8 (6)
$1C_{b6}$	3.3 (5)	7.4 (7)	9.0 (8)	−1.9 (5)	0.1 (5)	4.4 (6)
$1C_{b7}$	3.8 (5)	6.4 (6)	6.6 (6)	−1.3 (5)	0.6 (5)	3.5 (5)
$1C_{b8}$	3.2 (5)	7.9 (7)	6.6 (6)	−2.8 (5)	0.3 (5)	3.6 (5)
$1C_{m1}$	2.5 (4)	4.6 (5)	4.7 (5)	−1.3 (4)	−0.6 (4)	1.4 (4)
$1C_{m2}$	3.5 (5)	4.4 (5)	5.7 (6)	−0.7 (4)	−0.1 (4)	2.4 (4)
$1C_{m3}$	3.3 (5)	6.0 (6)	5.7 (6)	−0.8 (4)	0.0 (4)	2.9 (5)
$1C_{m4}$	3.4 (5)	5.2 (5)	6.5 (6)	−1.1 (4)	0.3 (4)	2.4 (5)
$1C_1$	4.1 (5)	4.1 (5)	4.3 (5)	−1.6 (4)	0.3 (4)	0.8 (4)
$1C_2$	3.1 (5)	4.2 (5)	5.2 (5)	−1.0 (4)	0.4 (4)	1.0 (4)
$1C_3$	3.5 (5)	6.0 (6)	5.5 (6)	−2.0 (4)	−0.5 (4)	0.5 (5)
$1C_4$	3.7 (6)	6.4 (7)	7.0 (7)	−1.5 (5)	0.0 (5)	1.0 (6)
$1C_5$	5.4 (7)	5.4 (6)	8.2 (7)	−1.6 (5)	−0.3 (6)	1.7 (5)
$1C_6$	3.6 (5)	5.9 (6)	5.5 (6)	−1.9 (5)	0.3 (4)	1.1 (5)
$1C_7$	3.3 (5)	5.6 (6)	7.2 (7)	−1.6 (4)	−0.9 (5)	3.7 (5)
$1C_8$	6.5 (7)	7.3 (7)	8.7 (8)	−3.4 (6)	−0.4 (6)	4.2 (6)
$1C_9$	7.5 (8)	11.0 (10)	9.8 (9)	−5.0 (8)	−1.0 (7)	6.0 (9)
$1C_{10}$	4.8 (7)	8.0 (9)	10.8 (11)	−2.0 (6)	−1.7 (7)	4.2 (8)
$1C_{11}$	6.7 (8)	7.8 (8)	12.1 (11)	−1.7 (6)	−0.1 (7)	6.0 (8)
$1C_{12}$	7.3 (7)	4.4 (6)	10.5 (9)	−0.9 (6)	−0.4 (6)	3.7 (6)
$1C_{13}$	1.9 (5)	10.6 (9)	7.6 (7)	−0.8 (6)	0.5 (5)	4.5 (7)
$1C_{14}$	5.2 (7)	11.9 (9)	6.2 (7)	−5.9 (7)	−1.3 (5)	3.6 (6)
$1C_{15}$	4.7 (7)	15.2 (13)	7.3 (8)	−4.8 (8)	−0.3 (6)	4.3 (8)
$1C_{16}$	4.7 (8)	16.2 (16)	9.5 (10)	−3.4 (9)	−0.9 (7)	7.5 (11)
$1C_{17}$	4.6 (8)	15.8 (14)	12.3 (12)	−1.6 (8)	1.4 (7)	7.9 (11)
$1C_{18}$	2.1 (5)	10.6 (9)	9.5 (8)	0.1 (6)	0.6 (5)	4.8 (7)
$1C_{19}$	2.3 (5)	5.2 (6)	7.6 (7)	−0.8 (4)	−0.3 (4)	3.5 (5)
$1C_{20}$	5.0 (6)	5.1 (6)	9.7 (8)	−1.3 (5)	−0.1 (5)	4.0 (6)
$1C_{21}$	6.7 (8)	9.4 (9)	13.3 (12)	−3.8 (7)	−3.5 (8)	6.1 (9)
$1C_{22}$	6.4 (8)	10.6 (11)	13.1 (13)	−2.8 (7)	0.3 (4)	6.4 (9)
$1C_{23}$	5.6 (7)	11.0 (10)	8.9 (9)	−0.4 (8)	1.0 (6)	5.5 (9)
$1C_{24}$	4.8 (6)	9.4 (8)	6.3 (7)	−1.0 (5)	0.7 (5)	4.0 (6)
2Fe	2.93 (7)	4.36 (7)	5.08 (8)	−1.27 (5)	−0.04 (5)	1.62 (6)
$2N_1$	3.1 (4)	4.3 (4)	5.5 (4)	−1.1 (3)	−0.2 (3)	1.4 (3)
$2N_2$	2.5 (4)	4.4 (4)	6.8 (5)	−0.8 (3)	−0.7 (3)	1.7 (3)
$2N_3$	3.3 (4)	4.9 (4)	5.8 (4)	−1.1 (3)	−0.8 (3)	2.5 (3)
$2N_4$	2.3 (3)	5.2 (4)	5.6 (4)	−0.4 (3)	0.5 (3)	2.2 (3)
$2C_{a8}$	3.8 (5)	4.8 (5)	4.6 (5)	−2.0 (4)	0.5 (4)	1.9 (4)
$2C_{a7}$	3.6 (5)	5.2 (5)	4.7 (5)	−1.0 (4)	−0.2 (4)	2.3 (4)
$2C_{a6}$	3.5 (5)	5.8 (6)	5.4 (6)	−1.2 (4)	−0.7 (4)	2.3 (5)
$2C_{a5}$	3.9 (5)	4.4 (5)	5.8 (6)	−1.3 (4)	0.3 (4)	1.8 (4)
$2C_{a4}$	3.5 (5)	5.0 (5)	6.4 (6)	−1.6 (4)	0.6 (4)	2.0 (4)
$2C_{a3}$	3.2 (5)	4.2 (5)	5.5 (5)	−0.9 (4)	0.3 (4)	1.8 (4)
$2C_{a2}$	3.2 (5)	4.0 (5)	5.6 (5)	−0.8 (4)	−0.3 (4)	1.2 (4)
$2C_{a1}$	2.8 (5)	4.0 (5)	5.3 (5)	−1.2 (4)	−0.4 (4)	1.4 (4)
$2C_{b8}$	3.4 (5)	6.4 (6)	7.0 (6)	−2.3 (5)	−1.2 (5)	1.7 (5)
$2C_{b7}$	4.0 (5)	6.3 (6)	7.3 (7)	−2.3 (5)	−0.1 (5)	3.7 (5)
$2C_{b6}$	4.7 (6)	5.1 (5)	6.5 (6)	−2.0 (5)	0.2 (5)	2.4 (5)
$2C_{b5}$	4.2 (6)	6.8 (6)	6.7 (6)	−1.4 (5)	−0.5 (5)	3.8 (5)
$2C_{b4}$	2.6 (5)	7.3 (7)	6.6 (6)	−1.2 (5)	0.9 (4)	1.3 (5)
$2C_{b3}$	4.3 (6)	5.4 (6)	8.0 (7)	−1.8 (5)	1.0 (5)	1.7 (5)
$2C_{b2}$	4.1 (6)	5.5 (6)	6.5 (6)	−2.1 (5)	−0.2 (5)	1.7 (5)
$2C_{b1}$	4.3 (6)	5.7 (6)	6.2 (6)	−1.2 (5)	−1.0 (5)	2.0 (5)
$2C_{m1}$	2.8 (5)	4.3 (5)	5.0 (5)	−1.3 (4)	−0.8 (4)	1.2 (4)
$2C_{m2}$	3.7 (5)	4.6 (5)	5.7 (6)	−1.7 (4)	−0.4 (4)	2.8 (4)
$2C_{m3}$	2.9 (5)	6.6 (6)	6.0 (6)	−2.0 (4)	−1.0 (5)	2.1 (5)
$2C_{m4}$	4.6 (6)	4.2 (5)	5.6 (6)	−1.8 (4)	−0.2 (4)	2.1 (4)
$2C_1$	4.0 (5)	4.6 (5)	4.8 (5)	−1.2 (5)	0.7 (4)	0.9 (4)
$2C_2$	3.6 (5)	4.8 (5)	4.4 (5)	−1.6 (4)	1.0 (4)	0.5 (4)
$2C_3$	2.9 (5)	5.7 (6)	6.0 (6)	−0.6 (4)	0.4 (4)	2.5 (5)

Table IV (*Continued*)

atom	B_{11}	B_{22}	B_{33}	B_{12}	B_{13}	B_{23}
$2C_4$	4.7 (6)	4.8 (6)	5.9 (6)	−1.3 (5)	0.6 (5)	1.3 (5)
$2C_5$	6.2 (7)	7.0 (7)	6.4 (7)	0.2 (6)	0.6 (6)	2.3 (6)
$2C_6$	3.9 (6)	5.2 (6)	6.2 (6)	0.1 (5)	0.3 (4)	1.6 (5)
$2C_7$	4.6 (6)	5.5 (6)	6.3 (7)	−1.8 (5)	0.0 (5)	2.3 (5)
$2C_8$	9.0 (9)	10.4 (9)	7.2 (8)	−4.9 (7)	0.5 (6)	4.0 (7)
$2C_9$	11.3 (11)	12.1 (11)	8.9 (10)	−5.3 (9)	1.0 (8)	4.9 (9)
$2C_{10}$	7.6 (9)	9.2 (9)	10.7 (11)	−3.0 (7)	0.4 (8)	4.5 (9)
$2C_{11}$	7.9 (8)	8.2 (8)	10.8 (10)	−3.6 (7)	−0.9 (8)	3.7 (8)
$2C_{12}$	6.6 (7)	5.9 (6)	7.1 (7)	−3.3 (5)	−0.3 (5)	2.4 (5)
$2C_{13}$	4.0 (6)	5.5 (6)	5.2 (6)	−2.1 (5)	−0.9 (5)	2.4 (5)
$2C_{14}$	5.0 (6)	7.2 (7)	7.0 (7)	−2.7 (5)	−2.9 (5)	2.7 (6)
$2C_{15}$	6.7 (8)	8.6 (8)	8.7 (8)	−2.2 (7)	−2.6 (7)	4.8 (7)
$2C_{16}$	4.1 (7)	8.5 (8)	11.1 (11)	−1.8 (6)	−1.8 (7)	5.1 (8)
$2C_{17}$	4.9 (7)	6.5 (7)	9.7 (9)	−2.1 (5)	−1.5 (6)	4.4 (7)
$2C_{18}$	2.4 (5)	6.4 (6)	9.5 (8)	−1.2 (4)	−0.2 (5)	3.9 (6)
$2C_{19}$	4.4 (6)	4.2 (5)	8.1 (7)	−2.2 (5)	−2.3 (5)	3.4 (5)
$2C_{20}$	6.2 (7)	7.0 (7)	8.6 (8)	−3.5 (6)	−2.1 (6)	4.8 (6)
$2C_{21}$	5.9 (8)	9.6 (9)	11.8 (11)	−3.2 (7)	−2.0 (7)	6.1 (9)
$2C_{22}$	7.3 (9)	11.4 (12)	10.9 (11)	−5.3 (9)	−3.8 (8)	7.0 (10)
$2C_{23}$	5.5 (7)	11.2 (10)	9.2 (9)	−4.4 (7)	−1.5 (6)	5.6 (8)
$2C_{24}$	3.1 (5)	10.5 (9)	7.6 (7)	−2.9 (6)	−0.9 (5)	4.4 (7)
O	2.7 (3)	5.4 (3)	6.7 (4)	−1.69 (26)	−0.40 (27)	1.7 (3)
N_{B_1}	3.7 (4)	3.9 (4)	6.1 (5)	−0.7 (4)	1.0 (4)	−0.4 (4)
N_{B_2}	3.6 (4)	4.7 (4)	5.5 (5)	−1.3 (4)	0.8 (3)	−0.6 (4)
C_B	4.7 (6)	4.0 (5)	5.0 (6)	−1.4 (5)	−0.9 (5)	1.2 (4)
O_B	2.8 (3)	6.1 (4)	9.2 (5)	−0.59 (29)	−1.2 (3)	0.9 (3)
W_1[b]	6.6 (7)	9.3 (8)	9.8 (8)	−1.5 (6)	−1.2 (6)	−0.2 (6)

[a] The B_{ij}'s are related to the dimensionless β_{ij}'s employed during refinement as $B_{ij} = 4\beta_{ij}/a_i^* a_j$. The estimated standard deviations of the least significant digits are given in parentheses. [b] W_1 is in the major occupancy water molecule. The oxygen atom of the minor occupancy water was refined isotropically. The final isotropic thermal parameter for W_2 is 4.9 (10).

thesized in a manner quite analogous to the iron and manganese homonuclear species but in our hands it could not be coerced into crystallizing cleanly.

The synthesis of $[MnCo(Im)(FF)]^-$ warrants comment as a rational method for obtaining a heteronuclear dimer. The only preparation which gave a respectable yield was that of treating the aminoporphyrin **1** with phosgene, adding 1 equiv of manganese premetalated aminoporphyrin to obtain the half-metalated face-to-face product, carefully chromatographing at this point, and finally, metalating with cobalt. Problems such as acid demetalation, trans-metalation, and chromatographic difficulties were experienced with all other routes and also with attempts to prepare other heteronuclear species. Similarly, other oxidation states of the metals used such as the highly desirable high-spin Fe(III) have so far proved intractable to clean synthesis and isolation with imidazolate ligation. Copper(II) porphyrins show little, if any, tendency to coordinate a fifth ligand and were not pursued for this reason (and also, the copper in cytochrome oxidase is not porphyrinic nor is it likely to have the strictly tetragonal structure dictated by a porphyrin).

Magnetic Susceptibility Studies. The magnetic moments of the four μ-imidazolate complexes **8–11** are essentially normal at room temperature. Thus, the ferrous Fe–Im–Fe and Fe–(2-MeIm)–Fe species have μ = 5.32 and 5.47 μ_B, respectively, per iron, expected for a high-spin five-coordinate S = 2 complex like Fe(2-MeImH)(TPP).[17] Similarly, the Mn–Im–Mn species has μ = 6.05 μ_B typical of a high-spin manganese(II) porphyrin in its preferred, five-coordinate geometry.[14] The Mn–Im–Co species **11** has a total room-temperature magnetic moment μ = 6.42 μ_B expected from a 1:1 mixture of an $S = {}^5/_2$ manganese(II) and an $S = {}^1/_2$ cobalt(II). These data alone speak to the lack of strong magnetic coupling via the imidazolate bridge but, as the detailed analysis of susceptibilities down to liquid-helium temperatures shows, all four complexes are weak antiferromagnets. The characteristic Néel temperature maxima are seen in Figures 1–3 for compounds **8–10** but not for **11** in Figure 4. This is because the latter $S = {}^5/_2, {}^1/_2$ system has a residual S = 2 system masking the coupling of two unpaired electrons. All four imidazolate species are found to have $-J$ in the range 2–5 cm^{-1}. This order of magnitude for $-J$ is greater than that observed in the low-spin imidazolate polymers $[M(Im)(TPP)]_n$ (M = Fe(III), Mn(III)) where it is essentially zero[11] but considerably smaller than that observed in copper imidazolate dimers where the range is 21–90 cm^{-1} (though most values cluster at the low end of the scale).[6,24,25] Without a substantial body of accurate structural data it is difficult to theorize on the causes of this wide range of values. However, a qualitative pattern is evident to us in the presently existing metalloporphyrin data, namely, detectable antiferromagnetic coupling across imidazolate requires mutual σ symmetry of the orbitals containing the unpaired electrons. This is possibly paralleled by results with copper dimers,[24] but the effect of the orientation of the imidazolate plane observed in other copper complexes[6] suggests that more subtle effects are dictating the precise magnitude of J. An increase in $|-J|$ seen in copper dimers when imidazolate is replaced by 2-methylimidazolate[24] is not paralleled by the same substitution in our diiron species **8** and **9**. Rather, they are identical within experimental error.

The oxo-bridged complex $Fe_2(\mu\text{-oxo})(FF)$ (**5**) is another of a large class of ferric dimers showing strong antiferromagnetic coupling.[26] Its value of $-J$, 107.5 cm^{-1} (see Figure 5), is a little lower than those of other hematin dimers which fall in the range 121–145 cm^{-1}. This is probably a result of greater departure from linearity of the Fe–O–Fe bond (161.4°) than in other hematin dimers (172.5–178.5°).[26–28] Repetition of the variable-temperature susceptibility measurements on **5** revealed a marked hysteresis in the data which we have traced to reversible loss of solvated water. Under vacuum near ambient temperatures the susceptibility was seen to decrease indicating an increase in the antiferromagnetic interaction. After air exposure of the sample overnight, the data were identical with those of an original sample. Infrared measurements (KBr disks) on samples treated in a similar fashion showed ν(OH) in **5** at 3350 cm^{-1} which disappeared upon heating under vacuum but reappeared (slightly broadened) upon exposure

(24) Haddad, M. S.; Hendrikson, D. N. *Inorg. Chem.* **1978**, *17*, 2622–2630.
(25) Hendriks, H. M. J.; Reedjik, J. *Inorg. Chim. Acta* **1979**, *37*, L509–510. Suzuki, M.; Kanatomi, H.; Koyama, H.; Murase, I. *Ibid.* **1980**, *44*, L41–L42.
(26) Murray, K. S. *Coord. Chem. Rev.* **1974**, *12*, 1–35.
(27) Hoffman, A. B.; Collins, C. M.; Day, V. W.; Fleischer, E. B.; Srivastava, T. S.; Hoard, J. L. *J. Am. Chem. Soc.* **1972**, *94*, 3620–3626.
(28) Radonovich, L. J.; Caughey, W. S.; Hoard, J. L., unpublished results.

Table VI. Selected Interatomic Distances (Å) for $Fe_2(\mu\text{-}O)FF\cdot H_2O$

1Fe-1N_1	2.040 (7)	1C_{10}-1C_{11}	1.341 (17)	2C_{b3}-2C_{b4}	1.392 (13)
1Fe-1N_2	2.106 (7)	1C_{11}-1C_{12}	1.400 (15)	2C_{b5}-2C_{b6}	1.362 (12)
1Fe-1N_3	2.052 (7)	1C_{m3}-1C_{13}	1.516 (13)	2C_{b7}-2C_{b8}	1.377 (12)
1Fe-1N_4	2.078 (7)	1C_{13}-1C_{14}	1.409 (15)	2C_{m1}-2C_1	1.520 (12)
1Fe-O	1.800 (6)	1C_{13}-1C_{18}	1.404 (15)	2C_1-2C_2	1.379 (12)
1N_1-1C_{a1}	1.384 (10)	1C_{14}-1C_{15}	1.434 (16)	2C_1-2C_6	1.404 (12)
1N_1-1C_{a2}	1.408 (10)	1C_{15}-1C_{16}	1.425 (20)	2C_2-2C_3	1.468 (12)
1N_2-1C_{a3}	1.410 (10)	1C_{16}-1C_{17}	1.343 (20)	2C_2-N_{B2}	1.372 (11)
1N_2-1C_{a4}	1.366 (10)	1C_{17}-1C_{18}	1.452 (17)	2C_3-2C_4	1.387 (13)
1N_3-1C_{a5}	1.377 (10)	1C_{m4}-1C_{19}	1.503 (12)	2C_4-2C_5	1.427 (14)
1N_3-1C_{a6}	1.409 (11)	1C_{19}-1C_{20}	1.407 (14)	2C_5-2C_6	1.450 (14)
1N_4-1C_{a7}	1.392 (11)	1C_{19}-1C_{24}	1.391 (14)	2C_{m2}-2C_7	1.496 (12)
1N_4-1C_{a8}	1.378 (10)	1C_{20}-1C_{21}	1.420 (15)	2C_7-2C_8	1.397 (14)
1C_{a1}-1C_{m4}	1.419 (12)	1C_{21}-1C_{22}	1.442 (19)	2C_7-2C_{12}	1.382 (13)
1C_{a1}-1C_{b1}	1.470 (12)	1C_{22}-1C_{23}	1.392 (18)	2C_8-2C_9	1.435 (16)
1C_{a2}-1C_{m1}	1.408 (11)	1C_{23}-1C_{24}	1.423 (16)	2C_9-2C_{10}	1.388 (18)
1C_{a2}-1C_{b2}	1.455 (12)	2Fe-2N_1	2.085 (7)	2C_{10}-2C_{11}	1.379 (17)
1C_{a3}-1C_{m1}	1.371 (11)	2Fe-2N_2	2.073 (7)	2C_{11}-2C_{12}	1.438 (15)
1C_{a3}-1C_{b3}	1.432 (11)	2Fe-2N_3	2.075 (7)	2C_{m3}-2C_{13}	1.505 (12)
1C_{a4}-1C_{m2}	1.386 (11)	2Fe-2N_4	2.088 (7)	2C_{13}-2C_{14}	1.392 (14)
1C_{a4}-1C_{b4}	1.436 (12)	2Fe-O	1.774 (6)	2C_{13}-2C_{18}	1.394 (13)
1C_{a5}-1C_{m2}	1.412 (12)	2N_1-2C_{a1}	1.383 (10)	2C_{14}-2C_{15}	1.435 (14)
1C_{a5}-1C_{b5}	1.455 (12)	2N_1-2C_{a2}	1.396 (10)	2C_{15}-2C_{16}	1.396 (17)
1C_{a6}-1C_{m3}	1.400 (12)	2N_2-2C_{a3}	1.356 (10)	2C_{16}-2C_{17}	1.356 (16)
1C_{a6}-1C_{b6}	1.429 (13)	2N_2-2C_{a4}	1.410 (10)	2C_{17}-2C_{18}	1.434 (14)
1C_{a7}-1C_{m3}	1.417 (12)	2N_3-2C_{a5}	1.381 (10)	2C_{m4}-2C_{19}	1.513 (12)
1C_{a7}-1C_{b7}	1.439 (12)	2N_3-2C_{a6}	1.383 (10)	2C_{19}-2C_{20}	1.396 (14)
1C_{a8}-2C_{m4}	1.407 (12)	2N_4-2C_{a7}	1.392 (10)	2C_{19}-2C_{24}	1.423 (14)
1C_{a8}-1C_{b8}	1.434 (12)	2N_4-2C_{a8}	1.383 (10)	2C_{20}-2C_{21}	1.451 (15)
1C_{b1}-1C_{b2}	1.345 (12)	2C_{a1}-2C_{m4}	1.417 (12)	2C_{21}-2C_{22}	1.371 (19)
1C_{b3}-1C_{b4}	1.354 (12)	2C_{a1}-2C_{b1}	1.469 (12)	2C_{22}-2C_{23}	1.401 (19)
1C_{b5}-1C_{b6}	1.336 (13)	2C_{a2}-2C_{m1}	1.368 (12)	2C_{23}-2C_{24}	1.424 (15)
1C_{b7}-1C_{b8}	1.358 (12)	2C_{a2}-2C_{b2}	1.430 (12)	N_{B1}-C_B	1.358 (11)
1C_{m1}-1C_1	1.506 (12)	2C_{a3}-2C_{m1}	1.378 (11)	N_{B1}-C_B	1.380 (11)
1C_1-1C_2	1.393 (12)	2C_{a3}-2C_{b3}	1.468 (12)	C_B-O_B	1.251 (11)
1C_1-1C_6	1.378 (12)	2C_{a4}-2C_{m2}	1.366 (12)	O-W_1	2.869 (13)
1C_2-1C_3	1.451 (12)	2C_{a4}-2C_{b4}	1.480 (12)	O-W_2	2.81 (4)
1C_2-N_{B1}	1.406 (11)	2C_{a5}-2C_{m2}	1.433 (12)	N_{B1}-W_1	3.041 (13)
1C_3-1C_4	1.377 (13)	2C_{a5}-2C_{b5}	1.434 (12)	N_{B1}-W_2	2.86 (4)
1C_4-1C_5	1.404 (14)	2C_{a6}-2C_{m3}	1.386 (12)	N_{B2}-W_1	2.824 (14)
1C_5-1C_6	1.439 (13)	2C_{a6}-2C_{b6}	1.474 (12)	N_{B2}-W_2	3.17 (4)
1C_{m2}-1C_7	1.503 (12)	2C_{a7}-2C_{m3}	1.389 (12)	W_1-H_{NB1}	2.32
1C_7-1C_8	1.423 (14)	2C_{a7}-2C_{b7}	1.410 (12)	W_1-H_{NB2}	2.09
1C_7-2C_{12}	1.371 (14)	2C_{a8}-2C_{m4}	1.393 (12)	W_2-H_{NB1}	2.15
1C_8-1C_9	1.438 (15)	2C_{a8}-2C_{b8}	1.452 (12)	W_2-H_{NB2}	2.50
1C_9-1C_{10}	1.432 (18)	2C_{b1}-2C_{b2}	1.384 (12)		

[a] The estimated standard deviations of the least significant digits are given in parentheses.

to air of ambient humidity. The X-ray crystal structure provides a ready explanation of these observations. The solvated water molecule which is H bonded to the bridging oxide is presumably lost under vacuum and heating. This perturbation of the Fe–O–Fe moiety, possibly allowing it to become more nearly linear, gives rise to a slight increase in the magnetic interaction. No attempt was made to quantify this change since probable accompanying toluene solvate loss complicated the formula weight assignment.

X-ray Structure. The structure of $Fe_2(\mu\text{-}O)(FF)\cdot H_2O$ is, in most respects, quite similar to the other three μ-oxo porphinato(III) oligomers of known structure ($[Fe(TPP)]_2O$,[27] $[Fe(ProtoMe_2)]_2O$,[28] and $[Fe(ODM)]_2O$).[29] All have coordination group geometries typical of high-spin five-coordinate iron(III).[30] The average Fe–O distance of 1.787 (18) Å in $Fe_2(\mu\text{-}O)(FF)\cdot H_2O$ is comparable to the 1.763-Å value in $[Fe(TPP)]_2O$, 1.752 Å in $[Fe(ODM)]_2O$, and ~1.73 Å in $[Fe(ProtoMe_2)]_2O$. The most significant differing structural feature is the Fe–O–Fe angle. In $Fe(\mu\text{-}O)(FF)\cdot H_2O$, this angle is 161.1 (4)°; in the other derivatives the Fe–O–Fe group is more nearly linear with values of 174.5 (1)° ($[Fe(TPP)]_2O$), 178.5 (6)° ($[Fe(ODM)]_2O$, and 172.5° ($[Fe(ProtoMe_2)]_2O$).

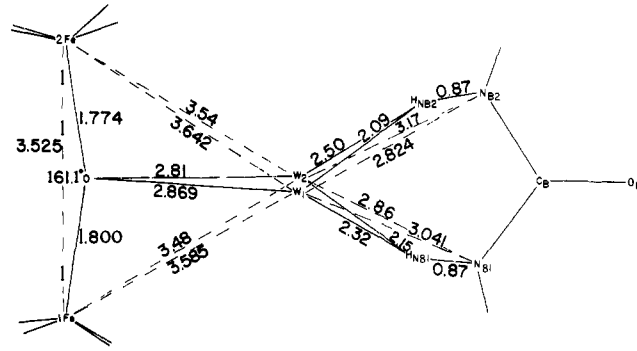

Figure 9. A scaled sketch displaying the manifold separations involving the major (W_1) and minor (W_2) water molecules and the Fe–O–Fe and urea bridges. The indicated positions of W_1 and W_2 have been arbitrarily separated for clarity. All distances are in units of angstroms.

The features that control the Fe–O–Fe angle in μ-oxo-iron(III) complexes are not well understood.[26] However, the ~140° angle found in three different crystalline forms of $[Fe(salen)]_2O$[31] does

(29) Kenny, J. F.; Scheidt, W. R.; Buchler, J. W., unpublished results.
(30) Scheidt, W. R. In "The Porphyrins"; Dolphin, D., Ed., Academic Press: New York, 1978; Vol. 3, pp 463–511. Hoard, J. L. In "Porphyrins and Metalloporphyrins"; Smith, K. M., Ed.; Elsevier: Amsterdam, 1975; pp 317–380.

(31) Gerloch, M.; McKenzie, E. D.; Towl, A. D. C. *J. Chem. Soc. A* **1969**, 2850–2858. Coggon, P.; McPhail, A. T.; Mabbs, F. E.; McLachlan, V. N. *Ibid.* **1971**, 1014–1019; Atovmyan, L. O.; D'yachenko, O. A.; Soboleva, S. V. *J. Struct. Chem. (Engl. Transl.)* **1970**, *11*, 517–518. Davies, J. E.; Gatehouse, B. M. *Acta Crystallogr., Sect. B* **1973**, *B29*, 1934–1942.

Table VII. Selected Interatomic Angles (Deg) for $Fe_2(\mu\text{-}O)FF\cdot H_2O$

$1N_1$-1Fe-$1N_2$	86.36 (28)	$2N_1$-2Fe-$2N_2$	85.10 (27)	$1C_{a8}$-$1C_{m4}$-$1C_{a1}$	123.9 (9)	$2C_{a8}$-$2C_{m4}$-$2C_{a1}$	124.2 (9)
$1N_1$-1Fe-$1N_3$	149.6 (3)	$2N_1$-2Fe-$2N_3$	149.8 (3)	$1C_{a2}$-$1C_{m1}$-$1C_{a3}$	125.2 (8)	$2C_{a2}$-$2C_{m1}$-$2C_{a3}$	125.9 (8)
$1N_1$-1Fe-$1N_4$	86.1 (3)	$2N_1$-2Fe-$2N_4$	86.35 (29)	$1C_{a4}$-$1C_{m2}$-$1C_{a5}$	124.3 (7)	$2C_{a4}$-$2C_{m2}$-$2C_{a5}$	123.5 (9)
$1N_1$-1Fe-O	105.21 (29)	$2N_1$-2Fe-O	104.69 (28)	$1C_{a6}$-$1C_{m3}$-$1C_{a7}$	125.9 (9)	$2C_{a6}$-$2C_{m3}$-$2C_{a7}$	125.0 (8)
$1N_2$-1Fe-$1N_3$	85.8 (3)	$2N_2$-2Fe-$2N_3$	86.7 (3)	$1C_{a2}$-$1C_{m1}$-$1C_1$	116.8 (8)	$2C_{a2}$-$2C_{m1}$-$2C_1$	119.9 (9)
$1N_2$-1Fe-$1N_4$	151.2 (3)	$2N_2$-2Fe-$2N_4$	148.9 (3)	$1C_{a3}$-$1C_{m1}$-$1C_1$	118.0 (8)	$2C_{a3}$-$2C_{m1}$-$2C_1$	114.2 (9)
$1N_2$-1Fe-O	106.39 (27)	$2N_2$-2Fe-O	102.72 (27)	$1C_{a4}$-$1C_{m2}$-$1C_7$	118.8 (8)	$2C_{a4}$-$2C_{m2}$-$2C_7$	117.0 (8)
$1N_3$-1Fe-$1N_4$	87.1 (3)	$2N_3$-2Fe-$2N_4$	85.83 (27)	$1C_{a5}$-$1C_{m2}$-$1C_7$	116.3 (7)	$2C_{a5}$-$2C_{m2}$-$2C_7$	119.4 (8)
$1N_3$-1Fe-O	105.21 (29)	$2N_3$-2Fe-O	105.48 (29)	$1C_{a6}$-$1C_{m3}$-$1C_{13}$	118.3 (9)	$2C_{a6}$-$2C_{m3}$-$2C_{13}$	117.7 (8)
$1N_4$-1Fe-O	101.80 (28)	$2N_4$-2Fe-O	108.36 (27)	$1C_{a7}$-$1C_{m3}$-$1C_{13}$	115.7 (8)	$2C_{a7}$-$2C_{m3}$-$2C_{13}$	117.1 (8)
1Fe-$1N_1$-$1C_{a1}$	126.4 (6)	2Fe-$2N_1$-$2C_{a1}$	124.4 (6)	$1C_{a8}$-$1C_{m4}$-$1C_{19}$	117.7 (8)	$2C_{a8}$-$2C_{m4}$-$2C_{19}$	117.4 (8)
1Fe-$1N_1$-$1C_{a2}$	127.9 (6)	2Fe-$2N_1$-$2C_{a2}$	126.6 (6)	$1C_{a1}$-$1C_{m4}$-$1C_{19}$	118.3 (8)	$2C_{a1}$-$2C_{m4}$-$2C_{19}$	118.4 (8)
1Fe-$1N_2$-$1C_{a3}$	125.7 (6)	2Fe-$2N_2$-$2C_{a3}$	129.2 (7)	$1C_{m1}$-$1C_1$-$1C_2$	119.5 (8)	$2C_{m1}$-$2C_1$-$2C_2$	121.7 (9)
1Fe-$1N_2$-$1C_{a4}$	126.6 (6)	2Fe-$2N_2$-$2C_{a4}$	122.8 (6)	$1C_{m1}$-$1C_1$-$1C_6$	118.4 (9)	$2C_{m1}$-$2C_1$-$2C_6$	117.3 (9)
1Fe-$1N_3$-$1C_{a5}$	127.3 (6)	2Fe-$2N_3$-$2C_{a5}$	124.7 (6)	$1C_6$-$1C_1$-$1C_2$	122.0 (9)	$2C_6$-$2C_1$-$2C_2$	121.0 (9)
1Fe-$1N_3$-$1C_{a6}$	127.7 (6)	2Fe-$2N_3$-$2C_{a6}$	127.1 (6)	$1C_1$-$1C_2$-$1C_3$	118.9 (8)	$2C_1$-$2C_2$-$2C_3$	119.8 (9)
1Fe-$1N_4$-$1C_{a7}$	127.6 (7)	2Fe-$2N_4$-$2C_{a7}$	129.6 (6)	$1C_1$-$1C_2$-N_{B1}	119.1 (8)	$2C_1$-$2C_2$-N_{B2}	117.5 (9)
1Fe-$1N_4$-$1C_{a8}$	126.4 (6)	2Fe-$2N_4$-$2C_{a8}$	125.2 (6)	$1C_2$-$1C_3$-$1C_4$	118.4 (9)	$2C_2$-$2C_3$-$2C_4$	118.7 (9)
$1C_{a1}$-$1N_1$-$1C_{a2}$	102.7 (7)	$2C_{a1}$-$2N_1$-$2C_{a2}$	105.2 (6)	$1C_3$-$1C_4$-$1C_5$	123.0 (9)	$2C_3$-$2C_4$-$2C_5$	122.2 (10)
$1C_{a3}$-$1N_2$-$1C_{a4}$	106.6 (7)	$2C_{a3}$-$2N_2$-$2C_{a4}$	107.3 (7)	$1C_3$-$1C_2$-N_{B1}	121.9 (8)	$2C_3$-$2C_2$-N_{B2}	122.6 (8)
$1C_{a5}$-$1N_3$-$1C_{a6}$	103.4 (7)	$2C_{a5}$-$2N_3$-$2C_{a6}$	105.5 (6)	$1C_4$-$1C_5$-$1C_6$	117.6 (10)	$2C_4$-$2C_5$-$2C_6$	117.5 (10)
$1C_{a7}$-$1N_4$-$1C_{a8}$	104.6 (7)	$2C_{a7}$-$2N_4$-$2C_{a8}$	105.2 (6)	$1C_5$-$1C_6$-$1C_1$	120.0 (9)	$2C_5$-$2C_6$-$2C_1$	120.5 (10)
$1N_1$-$1C_{a1}$-$1C_{m4}$	124.6 (8)	$2N_1$-$2C_{a1}$-$2C_{m4}$	124.1 (8)	$1C_{m2}$-$1C_7$-$1C_8$	118.0 (10)	$2C_{m2}$-$2C_7$-$2C_8$	120.6 (10)
$1N_1$-$1C_{a1}$-$1C_{b1}$	112.9 (8)	$2N_1$-$2C_{a1}$-$2C_{b1}$	110.1 (8)	$1C_{m2}$-$1C_7$-$1C_{12}$	121.6 (10)	$2C_{m2}$-$2C_7$-$2C_{12}$	116.8 (10)
$1C_{m4}$-$1C_{a1}$-$1C_{b1}$	122.4 (8)	$2C_{m4}$-$2C_{a1}$-$2C_{b1}$	125.4 (8)	$1C_{12}$-$1C_7$-$1C_8$	120.4 (10)	$2C_{12}$-$2C_7$-$2C_8$	122.6 (10)
$1N_1$-$1C_{a2}$-$2C_{m1}$	124.5 (8)	$2N_1$-$2C_{a2}$-$2C_{m1}$	123.9 (8)	$1C_7$-$1C_8$-$1C_9$	117.6 (12)	$2C_7$-$2C_8$-$2C_9$	118.2 (12)
$1N_1$-$1C_{a2}$-$1C_{b2}$	111.2 (8)	$2N_1$-$2C_{a2}$-$2C_{b2}$	111.6 (8)	$1C_8$-$1C_9$-$1C_{10}$	119.2 (13)	$2C_8$-$2C_9$-$2C_{10}$	119.3 (13)
$1C_{m1}$-$1C_{a2}$-$1C_{b2}$	124.3 (8)	$2C_{m1}$-$2C_{a2}$-$2C_{b2}$	124.4 (9)	$1C_9$-$1C_{10}$-$1C_{11}$	120.8 (13)	$2C_9$-$2C_{10}$-$2C_{11}$	121.7 (13)
$1N_2$-$1C_{a3}$-$2C_{m1}$	125.7 (8)	$2N_2$-$2C_{a3}$-$2C_{m1}$	125.0 (8)	$1C_{10}$-$1C_{11}$-$1C_{12}$	120.5 (14)	$2C_{10}$-$2C_{11}$-$2C_{12}$	119.8 (12)
$1N_2$-$1C_{a3}$-$1C_{b3}$	107.7 (8)	$2N_2$-$2C_{a3}$-$2C_{b3}$	111.7 (8)	$1C_{11}$-$1C_{12}$-$1C_7$	121.5 (12)	$2C_{11}$-$2C_{12}$-$2C_7$	118.2 (11)
$1C_{m1}$-$1C_{a3}$-$1C_{b3}$	126.5 (8)	$2C_{m1}$-$2C_{a3}$-$2C_{b3}$	123.2 (9)	$1C_{m3}$-$1C_{13}$-$1C_{14}$	119.4 (11)	$2C_{m3}$-$2C_{13}$-$1C_{14}$	118.8 (10)
$1N_2$-$1C_{a4}$-$1C_{m2}$	125.7 (8)	$2N_2$-$2C_{a4}$-$2C_{m2}$	128.1 (8)	$1C_{m3}$-$1C_{13}$-$1C_{18}$	115.2 (11)	$2C_{m3}$-$2C_{13}$-$2C_{18}$	119.4 (10)
$1N_2$-$1C_{a4}$-$1C_{b4}$	110.4 (8)	$2N_2$-$2C_{a4}$-$2C_{b4}$	108.0 (8)	$1C_{18}$-$1C_{13}$-$1C_{14}$	125.2 (10)	$2C_{18}$-$2C_{13}$-$2C_{14}$	121.8 (10)
$1C_{m2}$-$1C_{a4}$-$1C_{b4}$	123.9 (9)	$1C_{m2}$-$2C_{a4}$-$2C_{b4}$	123.8 (9)	$1C_{13}$-$1C_{14}$-$1C_{15}$	116.1 (13)	$2C_{13}$-$2C_{14}$-$2C_{15}$	118.2 (11)
$1N_3$-$1C_{a5}$-$1C_{m2}$	124.9 (8)	$2N_3$-$2C_{a5}$-$2C_{m2}$	123.4 (9)	$1C_{14}$-$1C_{15}$-$1C_{16}$	119.4 (14)	$2C_{14}$-$2C_{15}$-$2C_{16}$	120.3 (12)
$1N_3$-$1C_{a5}$-$1C_{b5}$	111.1 (8)	$2N_3$-$2C_{a5}$-$2C_{b5}$	111.8 (8)	$1C_{15}$-$1C_{16}$-$1C_{17}$	122.6 (15)	$2C_{15}$-$2C_{16}$-$2C_{17}$	120.3 (11)
$1C_{m2}$-$1C_{a5}$-$1C_{b5}$	123.9 (8)	$2C_{m2}$-$2C_{a5}$-$2C_{b5}$	124.4 (8)	$1C_{16}$-$1C_{17}$-$1C_{18}$	120.8 (16)	$2C_{16}$-$2C_{17}$-$2C_{18}$	121.3 (12)
$1N_3$-$1C_{a6}$-$1C_{m3}$	123.9 (9)	$2N_3$-$2C_{a6}$-$2C_{m3}$	126.2 (8)	$1C_{17}$-$1C_{18}$-$1C_{13}$	115.9 (13)	$2C_{17}$-$2C_{18}$-$2C_{13}$	118.1 (11)
$1N_3$-$1C_{a6}$-$1C_{b6}$	111.0 (8)	$2N_3$-$2C_{ab}$-$2C_{b6}$	109.2 (8)	$1C_{m4}$-$1C_{19}$-$1C_{20}$	115.7 (10)	$2C_{m4}$-$2C_{19}$-$2C_{20}$	118.4 (11)
$1C_{m3}$-$1C_{a6}$-$1C_{b6}$	125.2 (9)	$2C_{m3}$-$2C_{a6}$-$2C_{b6}$	124.6 (8)	$1C_{m4}$-$1C_{19}$-$1C_{24}$	120.4 (10)	$2C_{m4}$-$2C_{19}$-$2C_{24}$	118.6 (9)
$1N_4$-$1C_{a7}$-$1C_{m3}$	123.9 (8)	$2N_4$-$2C_{a7}$-$2C_{m3}$	123.8 (8)	$1C_{24}$-$1C_{19}$-$1C_{20}$	124.0 (10)	$2C_{24}$-$2C_{19}$-$2C_{20}$	122.9 (10)
$1N_4$-$1C_{a7}$-$1C_{b7}$	110.5 (9)	$2N_4$-$2C_{a7}$-$2C_{b7}$	111.1 (8)	$1C_{19}$-$1C_{20}$-$1C_{21}$	119.2 (12)	$2C_{19}$-$2C_{20}$-$2C_{21}$	119.3 (12)
$1C_{m3}$-$1C_{a7}$-$1C_{b7}$	125.5 (9)	$2C_{m3}$-$2C_{a7}$-$2C_{b7}$	125.0 (9)	$1C_{20}$-$1C_{21}$-$1C_{22}$	117.4 (14)	$2C_{20}$-$2C_{21}$-$2C_{22}$	117.4 (14)
$1N_4$-$1C_{a8}$-$1C_{m4}$	124.7 (8)	$2N_4$-$2C_{a8}$-$2C_{m4}$	126.6 (8)	$1C_{21}$-$1C_{22}$-$1C_{23}$	121.5 (14)	$2C_{21}$-$2C_{22}$-$2C_{23}$	123.3 (14)
$1N_4$-$1C_{a8}$-$1C_{b8}$	111.1 (8)	$2N_4$-$2C_{a8}$-$2C_{b8}$	111.0 (8)	$1C_{22}$-$1C_{23}$-$1C_{24}$	121.0 (14)	$2C_{22}$-$2C_{23}$-$2C_{24}$	120.6 (13)
$1C_{m4}$-$1C_{a8}$-$1C_{b8}$	123.9 (9)	$2C_{m4}$-$2C_{a8}$-$2C_{b8}$	123.1 (8)	$1C_{23}$-$1C_{24}$-$1C_{19}$	116.9 (12)	$2C_{23}$-$2C_{24}$-$1C_{19}$	116.1 (12)
$1C_{a1}$-$1C_{b1}$-$1C_{b2}$	105.2 (9)	$2C_{a1}$-$2C_{b1}$-$2C_{b2}$	106.5 (8)	$1C_2$-N_{B1}-C_B	129.6 (8)	$2C_2$-N_{B2}-C_B	129.6 (8)
$1C_{a2}$-$1C_{b2}$-$1C_{b1}$	108.0 (9)	$2C_{a2}$-$2C_{b2}$-$2C_{b1}$	106.5 (9)	N_{B1}-C_B-O_B	124.1 (9)	N_{B2}-C_B-O_B	124.0 (10)
$1C_{a3}$-$1C_{b3}$-$1C_{b4}$	109.0 (8)	$2C_{a3}$-$2C_{b3}$-$2C_{b4}$	105.3 (9)	1Fe-O-2Fe	161.1 (4)	N_{B1}-C_B-N_{B2}	111.8 (9)
$1C_{a4}$-$1C_{b4}$-$1C_{b3}$	106.4 (8)	$2C_{a4}$-$2C_{b4}$-$2C_{b3}$	107.6 (9)	1Fe-O-W_1	97.7 (3)	2Fe-O-W_1	100.7 (3)
$1C_{a5}$-$1C_{b5}$-$1C_{b6}$	106.8 (9)	$2C_{a5}$-$2C_{b5}$-$2C_{b6}$	106.2 (8)	1Fe-O-W_2	95.7 (9)	2Fe-O-W_2	98.8 (9)
$1C_{a6}$-$1C_{b6}$-$1C_{b5}$	107.5 (9)	$2C_{a6}$-$2C_{b6}$-$2C_{b5}$	107.2 (8)	O-W_1-H_{NB1}	109.5	O-W_2-H_{NB1}	117.3
$1C_{a7}$-$1C_{b7}$-$1C_{b8}$	106.7 (8)	$2C_{a7}$-$2C_{b7}$-$2C_{b8}$	107.2 (8)	O-W_1-H_{NB2}	117.2	O-W_2-H_{NB2}	106.3
$1C_{a8}$-$1C_{b8}$-$1C_{b7}$	107.0 (8)	$2C_{a8}$-$2C_{b8}$-$2C_{b7}$	106.3 (8)				

[a] The estimated standard deviations of the least significant digits are given in parentheses.

suggest that this linkage can exhibit considerable bending. The near linearity of the Fe–O–Fe moiety in the other porphyrin derivatives has been interpreted as the consequence of minimizing the nonbonded interactions between the porphinato cores. In $Fe_2(\mu\text{-}O)(FF)\cdot H_2O$, the decrease in the Fe–O–Fe angle is possibly associated with the formation of a hydrogen bond network between the oxo ligand, the water molecule, and the two N–H's of the urea link. A schematic diagram of the distances between these atoms is provided in Figure 9. The observed O···O(H_2O) separations of 2.81 and 2.87 Å and N–O(H_2O) separations of 2.86 and 2.82 Å are consistent with reasonably strong hydrogen bonds.[32] The location of the water molecule between the two porphinato planes, in what might be considered a hydrophobic region, suggests that the μ-oxo ligand atom must be reasonably basic in character. The structure thus offers a mechanistic suggestion of how ligand exchange with water might proceed.

It is possible that the bent Fe–O–Fe grouping is the consequence of accommodating the two porphinato cores linked by the urea bridge. The observed conformation leads to a N_{B1}–C_B–N_{B2} angle of 111.8° which is considerably smaller than that normally observed (116–118°) for urea[33] and substituted ureas.[34] The decrease in the N–C–N angle does permit a closer approach or "closing" of the two porphinato halves needed for the μ-oxo linkage. On the other hand, the interplanar separation at the ring periphery opposite the urea bridge would be slightly increased by a linear Fe–O–Fe group. We thus regard conformational effects as an unlikely reason for the 161° Fe–O–Fe angle and favor instead the effect of the H-bonded water molecule. An examination of Figure 7 suggests that "opening" the two porphinato

(32) Hamilton, W. C.; Ibers, J. A. "Hydrogen Bonding in Solids"; W. A. Benjamin: New York, 1968.

(33) Caron, A.; Donohue, J. *Acta Crystallogr., Sect. B* **1969**, *B25*, 404.
(34) Kashino, S.; Haisa, M. *Acta Crystallogr., Sect. B* **1977**, *B33*, 855–860. Huiszoon, C.; Tiemessen, G. W. M. *Ibid.* **1976**, 1604–1606. Tel, R. M.; Engberts, J. B. F. N. *J. Chem. Soc., Perkin Trans. 2* **1976**, 483–488.

halves, needed for binding a larger bridging ligand, would be as readily or more readily achieved than the "closed" conformation observed in $Fe_2(\mu\text{-}O)(FF)\cdot H_2O$. In particular, the separation of 6.4 Å between planes required[11] for a bridging imidazolate should be readily achieved.

Cytochrome Oxidase Relevance. The mixed-metal species $[MnCo(Im)(FF)]^-$ (**11**) is a good spin model for cytochrome oxidase.[7] Not only does it have interacting first-row transition-metal centers with $S = {}^5/_2$ and $S = {}^1/_2$ spin states like heme a_3 and Cu_B but also it has its unpaired electrons in an orbital orientation which is likely to exist in cytochrome oxidase. High-spin Mn(II) is isoelectronic with high-spin Fe(III) both having single occupation of all five 3d orbitals. Cobalt(II) is low spin having one unpaired electron in the d_{z^2} orbital, an antibonding orbital of σ symmetry with respect to Co-Im bonding. If present in an oxidase, an imidazolate ligand to Cu_B^{II} is likely to be the strongest field ligand[11] and therefore, by the fundamental premise of ligand field theory, would have the unpaired electron of the d^9 copper(II) ion in an orbital which is σ antibonding with respect to Cu-Im bonding. Thus, complex **11** would seem to be set up to maximize the antiferromagnetic coupling. But the measured value of $-J$ is only 5 cm^{-1}. This leads to the conclusion that a heme-Im-Cu structure like that envisaged for cytochrome oxidase is very unlikely to have $-J \geq 200$ cm^{-1}. Solution EPR studies on a proposed Fe-(2-MeIm)-Cu system are also consistent with very weak interactions.[35] The present range of $-J$ for all known imidazolate-bridged species is 0-90 cm^{-1}, so it is unlikely that histidine is providing a bridging ligand to Cu_B at the heme a_3 site of cytochrome oxidase. Other ligands which bring the metals closer together and which are known to mediate stronger antiferromagnetic coupling must be considered.

The structure of $Fe_2(\mu\text{-}O)(FF)$ is suggestive of an oxo-bridged Fe-O-Cu moiety in cytochrome oxidase, and we have adopted this as an alternative working hypothesis to the imidazolate model.[7] Oxygen-bridged moieties, in one form or another, have been frequently postulated in mechanisms involving oxygen reduction at dinuclear metal sites,[36] and the synthetic challenge of preparing heterobinuclear bridged oxo species seems worthy of future effort.

Acknowledgment. We are most grateful to Dr. Frank DiSalvo for variable-temperature magnetic susceptibility measurements and helpful discussions of the results. The work was supported by the National Institutes of Health, Grant GM 23851 to C.A.R. and Grant HL 15627 to W.R.S. J.T.L. was the recipient of an IntraScience Foundation Award. C.A.R. is a Camille and Henry Dreyfus Teacher-Scholar Awardee (1976-1981).

Supplementary Material Available: Table I, giving molar susceptibility and magnetic moment data for complexes **5**, **8**, **9**, and **11**, Table V, root-mean-square displacements of the atoms, a table of observed and calculated structure factor amplitudes (×10), and Table VIII, final group parameters and derived atomic coordinates for the toluene molecules (47 pages). Ordering information is given on any current masthead page.

(35) Prosperi, T.; Tomlinson, A. A. G. *J. Chem. Soc., Chem. Commun.* **1979**, 196-197.

(36) (a) Winfield, M. E. *Oxidases and Related Redox Systems, Proc. Symp.* **1965**, *1*, 115-130. (b) Bennet, L. E. *Prog. Inorg. Chem.* **1973**, *18*, 1-176. (c) Chance, B.; Saronio, C.; Leigh, J. S. *Proc. Natl. Acad. Sci. U.S.A.* **1975**, *72*, 1635-1640. (d) Blumberg, W. E.; Peisach, J. In "Cytochrome Oxidase"; King, T. E., Ed.; Elsevier/North-Holland Biomedical Press: Amsterdam, 1979; 153-159. (e) Wilson, D. F.; Erecińska, M. *Ibid.*, 315-318. (f) Caughey, W. S.; Wallace, W. J.; Volpe, J. A.; Yoshikawa, S. In "The Enzymes"; Boyer, P. D., Ed.; Academic Press: New York, 1976; Vol XIII, pp 299-344.

Migratory Insertion Reactions of Carbenes. Kinetics and Mechanism of Migratory Insertion Reactions of Zirconoxy Carbene Complexes of Niobocene Hydride and Alkyls

Richard S. Threlkel[1] and John E. Bercaw*[2]

Contribution No. 6272 from the Arthur Amos Noyes Laboratory of Chemical Physics, California Institute of Technology, Pasadena, California 91125. *Received July 21, 1980*

Abstract: Zirconoxy carbene complexes of niobocene hydride, phenyl, and alkyls, $(\eta^5\text{-}C_5H_5)_2(R)Nb{=}CHOZr(H)(\eta^5\text{-}C_5Me_5)_2$ (R = H, CH_3, $CH_2C_6H_5$, $CH_2C_6H_4OCH_3$, C_6H_5, $CH_2OZr(H)(\eta^2\text{-}C_5Me_5)_2$), are prepared via treatment of the corresponding niobocene carbonyls $(\eta^5\text{-}C_5H_5)_2Nb(CO)R$ with $(\eta^5\text{-}C_5Me_5)_2ZrH_2$. For R = H the rate (30.9 ± 1.8 s^{-1} at 32.5 °C) of tautomerization to $(\eta^5\text{-}C_5H_5)_2NbCH_2OZr(H)(\eta^5\text{-}C_5Me_5)_2$ was measured by using spin-saturation-transfer techniques (^1H NMR). The rates for alkyl migration to the zirconoxy carbene were obtained from the kinetics of the reactions with diphenylacetylene at 50 °C yielding $(\eta^5\text{-}C_5H_5)_2Nb(H)(PhC{\equiv}CPh)$ and the corresponding *trans*-enolate hydride complexes of bis(pentamethylcyclopentadienyl)zirconium(IV) $(\eta^5\text{-}C_5Me_5)_2Zr(H)(OCH{=}CHR')$. The relative migratory aptitudes ($H \gg CH_3 > CH_2C_6H_6OCH_3 > CH_2C_6H_5$) are discussed.

Introduction

The reduction of carbon monoxide by transition-metal hydrides is an area of intense current interest. We have been investigating the mechanism of CO hydrogenation with carbonyl and hydride derivatives of bis(pentamethylcyclopentadienyl)zirconium. Our findings are discussed in a recent review.[3] A key unsettled issue concerns the molecularity of the initial hydride transfer to the carbonyl ligand of $Cp^*_2ZrH_2(CO)$ ($Cp^* = \eta^5\text{-}C_5(CH_3)_5$) (**2**). Two plausible possibilities are (a) intramolecular insertion of CO into a Zr-H bond to yield $Cp^*_2Zr(H)(\eta^2\text{-}CHO)$ (**3**) which is subsequently reduced by $Cp^*_2ZrH_2$ (**1**) to $Cp^*_2(H)ZrCH_2OZr(H)Cp^*_2$

(1) Fannie and John Hertz Foundation Fellow, 1977-1980.
(2) Camille and Henry Dreyfus Teacher-Scholar, 1977-1982.

(3) (a) Manriquez, J. M.; McAlister, D. R.; Sanner, R. D.; Bercaw, J. E. *J. Am. Chem. Soc.* **1976**, *98*, 6733. (b) Wolczanski, P. T.; Bercaw, J. E. *Acc. Chem. Res.* **1980**, *13*, 121.

0002-7863/81/1503-2650$01.25/0